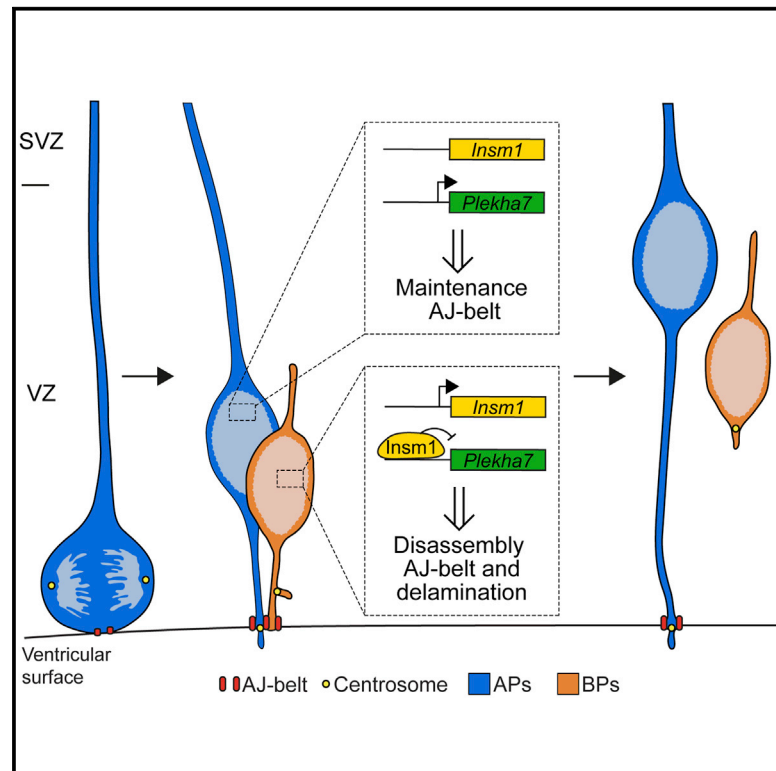


Neuron

Insm1 Induces Neural Progenitor Delamination in Developing Neocortex via Downregulation of the Adherens Junction Belt-Specific Protein Plekha7

Graphical Abstract



Authors

Stefania Tavano, Elena Taverna,
Nereo Kalebic, ...,
Michaela Wilsch-Bräuninger,
Judith T.M.L. Paridaen,
Wieland B. Huttner

Correspondence

j.t.m.l.paridaen@umcg.nl (J.T.M.L.P.),
huttner@mpi-cbg.de (W.B.H.)

In Brief

Tavano et al. identify a novel molecular mechanism underlying neural progenitor delamination from the ventricle, a prerequisite to form the subventricular zone, the germinal layer implicated in neocortex expansion. Downregulation of adherens-junction belt-specific protein Plekha7 is central to this mechanism.

Highlights

- Transcription repressor Insm1 promotes progenitor delamination in embryonic neocortex
- Insm1 converts apical radial glia to basal radial glia
- Adherens junction belt-specific protein Plekha7 is a major target of Insm1
- Downregulation of Plekha7 expression promotes cortical progenitor delamination



Insm1 Induces Neural Progenitor Delamination in Developing Neocortex via Downregulation of the Adherens Junction Belt-Specific Protein *Plekha7*

Stefania Tavano,¹ Elena Taverna,^{1,3} Nereo Kalebic,¹ Christiane Haffner,¹ Takashi Namba,¹ Andreas Dahl,² Michaela Wilsch-Bräuninger,¹ Judith T.M.L. Paridaen,^{1,4,*} and Wieland B. Huttner^{1,5,*}

¹Max Planck Institute of Molecular Cell Biology and Genetics, Pfotenhauerstraße 108, 01307 Dresden, Germany

²Deep Sequencing Group SFB 655, DFG Research Center for Regenerative Therapies and Biotechnology Center, Technische Universität Dresden, Fetscherstrasse 105, 01307 Dresden, Germany

³Present address: Department of Evolutionary Genetics, Max Planck Institute for Evolutionary Anthropology, Deutscher Platz 6, 04103 Leipzig, Germany

⁴Present address: European Research Institute for the Biology of Ageing, University Medical Center Groningen, 9713 AV Groningen, Netherlands

⁵Lead Contact

*Correspondence: j.t.m.l.paridaen@umcg.nl (J.T.M.L.P.), huttner@mpi-cbg.de (W.B.H.)

<https://doi.org/10.1016/j.neuron.2018.01.052>

SUMMARY

Delamination of neural progenitor cells (NPCs) from the ventricular surface is a crucial prerequisite to form the subventricular zone, the germinal layer linked to the expansion of the mammalian neocortex in development and evolution. Here, we dissect the molecular mechanism by which the transcription factor *Insm1* promotes the generation of basal progenitors (BPs). *Insm1* protein is most highly expressed in newborn BPs in mouse and human developing neocortex. Forced *Insm1* expression in embryonic mouse neocortex causes NPC delamination, converting apical to basal radial glia. *Insm1* represses the expression of the apical adherens junction belt-specific protein *Plekha7*. CRISPR/Cas9-mediated disruption of *Plekha7* expression suffices to cause NPC delamination. *Plekha7* overexpression impedes the intrinsic and counteracts the *Insm1*-induced, NPC delamination. Our findings uncover a novel molecular mechanism underlying NPC delamination in which a BP-genic transcription factor specifically targets the integrity of the apical adherens junction belt, rather than adherens junction components as such.

INTRODUCTION

A key question pertaining to the evolutionary expansion of the mammalian neocortex (Ncx) is, what are the rate-limiting factors that curtail the number of neurons generated during cortical development, and how can these be overcome? The neurons generated in the developing Ncx originate from neural progenitor cells (NPCs). The primary NPCs are the neuroepithelial cells and the apical radial glia (aRG) into which the former cells transform

with the onset of cortical neurogenesis, collectively referred to as apical progenitors (APs) (Taverna et al., 2014). The cell bodies of APs form the primary germinal layer of the developing Ncx, the ventricular zone (VZ).

It is a key cell biological feature that curtails the ability of APs to generate neurons in the numbers found in the Ncx. Specifically, APs exhibit epithelial characteristics, including apical-basal cell polarity, a basal process contacting the basal lamina, integration into an apical adherens junction (AJ) belt, and an apical plasma membrane that shows a canonical epithelial feature—an apical primary cilium (Taverna et al., 2014). The primary cilium persists throughout interphase and is only (partly) disassembled and endocytosed as a ciliary remnant when APs enter mitosis (Taverna et al., 2014). Due to this behavior of the primary cilium, the cilium's basal body, that is, the older centrosome and, after duplication, the younger centrosome is tethered to the apical plasma membrane during AP interphase (Taverna et al., 2014). As a consequence, the onset of AP mitosis, which requires the nucleus to be in close proximity to the centrosomes, typically occurs at, or very near to, the ventricular surface (VS), confining AP mitoses to the apical-most region of the VZ (Taverna et al., 2014). However, the limited space at the VS is insufficient to allow AP mitoses to take place, during the period of neurogenesis, in the numbers required to generate the neurons found in the Ncx (Taverna et al., 2014).

This limitation is overcome by aRG generating, rather than neurons, a secondary class of NPCs, the basal progenitors (BPs) (Taverna et al., 2014). BPs translocate their nuclei and cell bodies away from the VS in the basal direction and beyond the basal boundary of the VZ, establishing a second germinal zone, the subventricular zone (SVZ). Newborn BPs re-establish their primary cilium on the lateral, rather than apical, plasma membrane (Wilsch-Bräuninger et al., 2016). This enables the BP centrosomes to translocate, like the BP nucleus, basally to the SVZ, allowing BP mitosis to occur there. Importantly, BP mitoses, in contrast to the AP mitoses in the VZ, are not confined to any particular region of the SVZ. Compared to APs, this endows BPs with a huge advantage with regard to maximizing



the number of mitoses, as the SVZ can grow in thickness to accommodate an increasing number of mitotically active BPs. In fact, the evolutionary expansion of the Ncx has been linked to an increase in the pool size and proliferative capacity of BPs, and hence to a thickening of the SVZ (Lui et al., 2011; Florio and Huttner, 2014; Fernández et al., 2016).

Two main types of BPs can be distinguished, based on their morphology during M-phase: (1) basal intermediate progenitors (bIPs), which lack major processes at mitosis, and (2) basal radial glia (bRG), which exhibit basal and/or apical processes throughout their cell cycle including mitosis (Taverna et al., 2014). The latter BP type has been characterized following the identification and description of the outer SVZ (OSVZ) as the crucial germinal zone for cortical neuron production and Ncx expansion and is thought to be key for these processes (Lui et al., 2011; Florio and Huttner, 2014; Fernández et al., 2016). Moreover, the basal processes of bRG, in particular, have been attributed a pivotal role for the folding (gyrification) of the Ncx, by providing a fan-like scaffold for neuron migration to the cortical plate (CP) (Fernández et al., 2016).

Besides the translocation of their nuclei and centrosomes to the SVZ for mitosis, another major change in a key cell biological feature facilitates BPs to exploit their full potential as NPCs—the loss of ventricular contact and of integration into the apical AJ belt, a process referred to as delamination (Wilsch-Bräuninger et al., 2016). Indeed, both bIPs and bRG are known to undergo delamination, either during their generation from aRG in the course of aRG cytokinesis, or following their generation. In the former case, an oblique aRG cleavage plane results in one daughter cell being born without apical plasma membrane and without being integrated into the apical AJ belt (Taverna et al., 2014). In the latter case, a vertical aRG cleavage plane yields daughter cells, both of which are born with apical plasma membrane and being integrated into the apical AJ belt; subsequently, one (asymmetric aRG division) or both (symmetric consumptive aRG division) of these daughter cells retract the apical process from the VS and disengage from the apical AJ belt (Wilsch-Bräuninger et al., 2016).

Despite significant recent progress (Roussou et al., 2012; Niola et al., 2012; Itoh et al., 2013; Das and Storey, 2014), our understanding of the molecular mechanism underlying the disengagement of the NPC apical process from the apical AJ belt, which constitutes a requirement for its retraction from the VS, is still largely incomplete. In light of the crucial role of NPC delamination in the formation of the SVZ and for the expansion of the Ncx in development and evolution, we have here dissected this process in mouse embryos, exploiting our previous finding that Insulinoma-associated 1 (*Insm1*), a zinc-finger transcription factor belonging to the SNAG family, promotes the generation of BPs (Farkas et al., 2008).

RESULTS

In Mouse and Human, Developing Ncx *Insm1* Protein Is Most Highly Expressed in the Newborn BPs that Are Still Located in the VZ

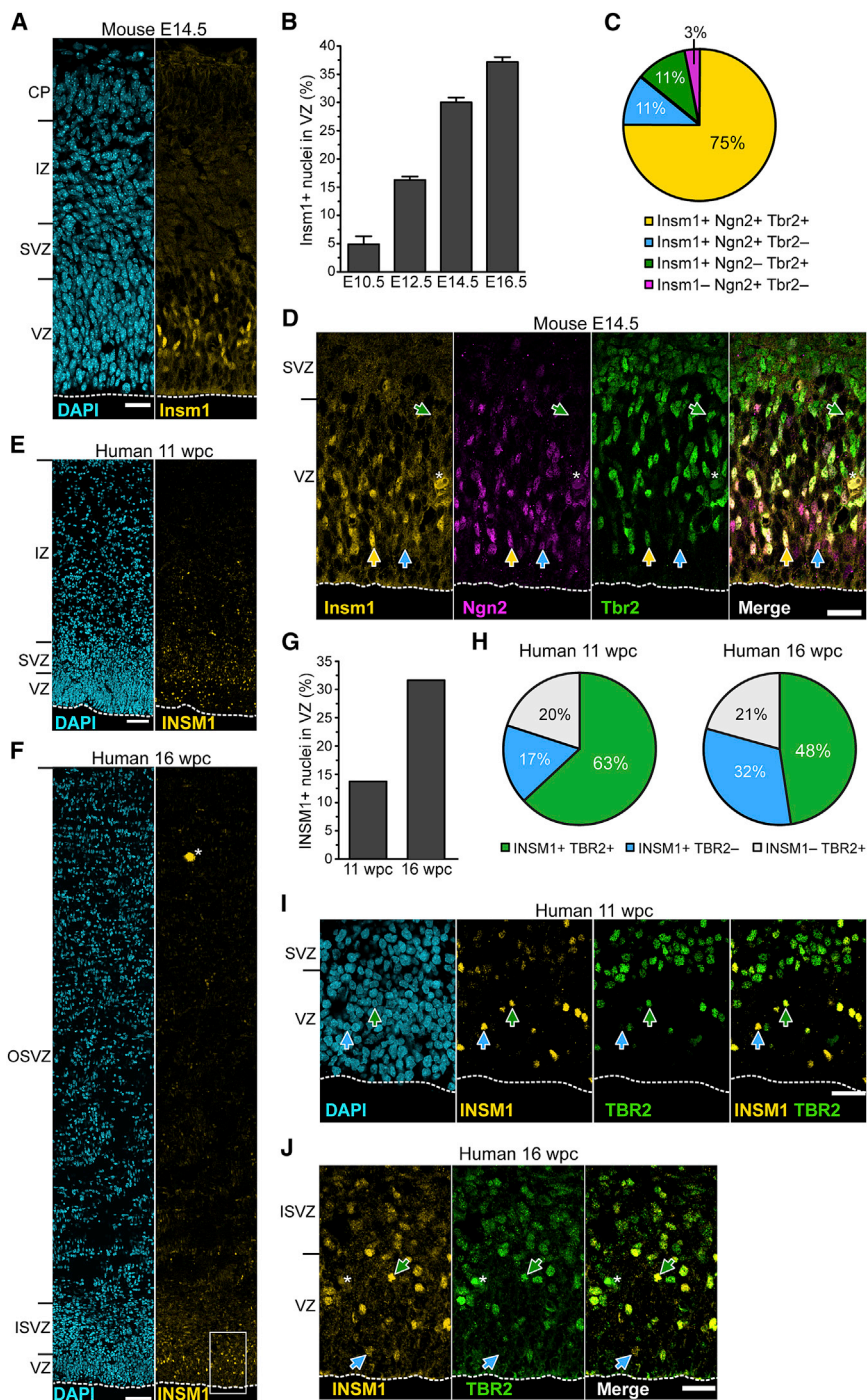
In the embryonic mouse and fetal human Ncx, the *Insm1* mRNA has previously been shown to be expressed in the germinal

zones, with the levels being higher in the SVZ than the VZ (Farkas et al., 2008; Fietz et al., 2012). However, differences in the mRNA versus protein levels between VZ and SVZ and among different NPC populations have been noted for other proteins implicated in BP generation, notably the transcription factor *Tbr2* (Fietz et al., 2012; Florio et al., 2015). We therefore examined the expression of the *Insm1* protein in developing mouse Ncx and placed the results obtained into context with the known distribution of the *Insm1* mRNA (Farkas et al., 2008; Fietz et al., 2012). Given that *Insm1* mRNA expression starts at the onset of neurogenesis (Farkas et al., 2008), we analyzed the protein expression at four stages of mouse Ncx development (E10.5, E12.5, E14.5, and E16.5), from the onset of neurogenesis until late neurogenesis (Figures 1A and S1A–S1C). *Insm1* protein was found to be most highly expressed in a subset of nuclei (from here on referred to as *Insm1*^{high} nuclei) present in the VZ and at much lower levels in nuclei in the SVZ (Figures 1A and S1A–S1C). The percentage of *Insm1*⁺ nuclei in the VZ increased during neurogenesis (Figure 1B), in line with the known increase in the proportion of NPCs in the VZ committed to neurogenesis (Taverna et al., 2014). These results show that the level of *Insm1* protein expression in the mouse VZ and SVZ differs from that of the mRNA and suggested that the primary function of *Insm1* may be exerted in the VZ.

We next sought to obtain evidence showing that the *Insm1*⁺ cells in the mouse VZ are newborn BPs by co-immunofluorescence (IF) for the BP markers *Ngn2* and *Tbr2* (Figures 1C and 1D). Quantification at mid-neurogenesis (E14.5) showed that the vast majority (>75%) of the *Insm1*⁺ nuclei in the VZ were positive for both BP markers, with the remainder of the *Insm1*⁺ VZ nuclei being positive for one or the other BP marker; only very few VZ nuclei positive for a BP marker were *Insm1*[−] (Figure 1C; for the distribution of the nuclei of the four subgroups along the radial axis, see Figure S1D). We conclude that all of the *Insm1*⁺ cells in the mouse VZ are newborn BPs.

In light of these results, and given that *Insm1* promotes the generation of BPs (Farkas et al., 2008), we next asked whether the VZ > SVZ pattern of *Insm1* protein expression is also conserved in fetal human Ncx. Indeed, *INSM1*^{high} nuclei were largely confined to the human VZ both at 11 and 16 weeks post-conception (wpc) (Figures 1E, 1F, and S2A–S2E). In contrast, in the human SVZ, notably the OSVZ, the level of expression of the *INSM1* protein was generally lower than in the human VZ (Figures 1E, 1F, and S2A–S2E). Similar to what was observed in the mouse developing Ncx, the percentage of *INSM1*⁺ nuclei in the human VZ increased during neurogenesis (Figure 1G). In particular, we observed a >2-fold increase in *INSM1*⁺ cells in the VZ from 11 (14%) to 16 (32%) wpc. These data not only show that also, for fetal human Ncx, the level of *INSM1* protein expression in the VZ and SVZ differs from that of the mRNA (see Fietz et al., 2012), but also indicate that the VZ > SVZ pattern of *Insm1* protein expression is conserved between mouse and human developing Ncx.

We therefore investigated whether also for human developing Ncx, the *INSM1*⁺ cells in the VZ were newborn BPs. Indeed, at both 11 and 16 wpc, the majority of the *INSM1*⁺ VZ nuclei were also *TBR2*⁺ (Figure 1H). However, quantification of the VZ nuclei that were *INSM1*⁺ and/or *TBR2*⁺ revealed that the



percentage of nuclei that were INSM1⁺ TBR2⁺ decreased during neurogenesis (from 63% at 11 wpc to 48% at 16 wpc) with a corresponding increase of INSM1⁺ TBR2⁻ (from 17% to 32%) but not of TBR2⁺ INSM1⁻ nuclei (Figure 1H). Furthermore, we found that >40% of the INSM1⁺ cells in the VZ expresses the radial glial marker HOPX (Nowakowski et al., 2016) (Figures S2F–S2I). These data are consistent with the greater complexity of BP subtypes in human than mouse developing

Ncx, in particular, with the possibility that the INSM1⁺ but TBR2⁻ cells in the VZ are newborn bRG.

Forced Insm1 Expression in APs Causes an Increase in Neurogenic BPs

If the Insm1⁺ nuclei that are increasingly observed in the VZ during the progression of cortical neurogenesis (Figure 1B) are newborn BPs, and in light of the previous finding that forced

Figure 1. Insm1 Protein in Mouse and Human Developing Ncx Is Most Highly Expressed by Newborn BPs in the VZ

(A) Insm1 IF (yellow) and DAPI staining (cyan) of E14.5 mouse Ncx.

(B) The percentage of VZ nuclei that are Insm1⁺ at the indicated stages of mouse Ncx development. See also Figures S1A–S1C.

(C) Nuclei in the E14.5 mouse VZ were examined for the presence of Insm1, Ngn2, and/or Tbr2. Four subpopulations were observed: Insm1⁺ Ngn2⁺ Tbr2⁺ (yellow), Insm1⁺ Ngn2⁺ Tbr2⁻ (blue), Insm1⁺ Ngn2⁻ Tbr2⁺ (green), and Insm1⁻ Ngn2⁺ Tbr2⁻ (magenta). Number of nuclei in each of the four subpopulations is expressed as percentage of the number of nuclei in the sum of the four subpopulations. See also Figure S1D.

(D) Insm1 (yellow), Ngn2 (magenta), and Tbr2 (green) triple IF of E14.5 mouse Ncx. Yellow arrows, Insm1⁺ Ngn2⁺ Tbr2⁺ nucleus; blue arrows, Insm1⁺ Ngn2⁺ Tbr2⁻ nucleus; green arrows, Insm1⁺ Ngn2⁻ Tbr2⁺ nucleus.

(E) Insm1 IF (yellow) and DAPI staining (cyan) of 11 wpc human fetal Ncx.

(F) Insm1 IF (yellow) and DAPI staining (cyan) of 16 wpc human fetal Ncx. Box indicates region shown at higher magnification in (J).

(G) The percentage of nuclei in the 11 wpc (left column) and 16 wpc (right column) human VZ that are Insm1⁺.

(H) The percentage of nuclei in the 11 wpc (left pie chart) and 16 wpc (right pie chart) human VZ that are either Insm1⁺ Tbr2⁺ (green), Insm1⁺ Tbr2⁻ (blue), or Insm1⁻ Tbr2⁺ (light gray). See also Figure S2.

(I) Insm1 (yellow) and Tbr2 (green) double IF and DAPI staining (cyan) of 11 wpc human fetal Ncx. Green arrows, Insm1⁺ Tbr2⁺ nucleus; blue arrows, Insm1⁺ Tbr2⁻ nucleus.

(J) Insm1 (yellow) and Tbr2 (green) double IF of 16 wpc human fetal Ncx of boxed region in (F). Green arrows, Insm1⁺ Tbr2⁺ nucleus; blue arrows, Insm1⁺ Tbr2⁻ nucleus.

In (A), (D)–(F), (I), and (J), all images are single 1- μ m optical sections. VS. Scale bars, 25 (A, D, I, and J) and 75 (E and F) μ m. Asterisks, IF artifact in (F) and autofluorescent blood vessels in (D) and (J). In (B), (C), (G), and (H), data are the mean of 3 independent experiments with 1 embryo per experiment in (B) and (C), and of 3–4 different cryosections from the same human fetal Ncx in (G) and (H). Error bars in (B), SEM.

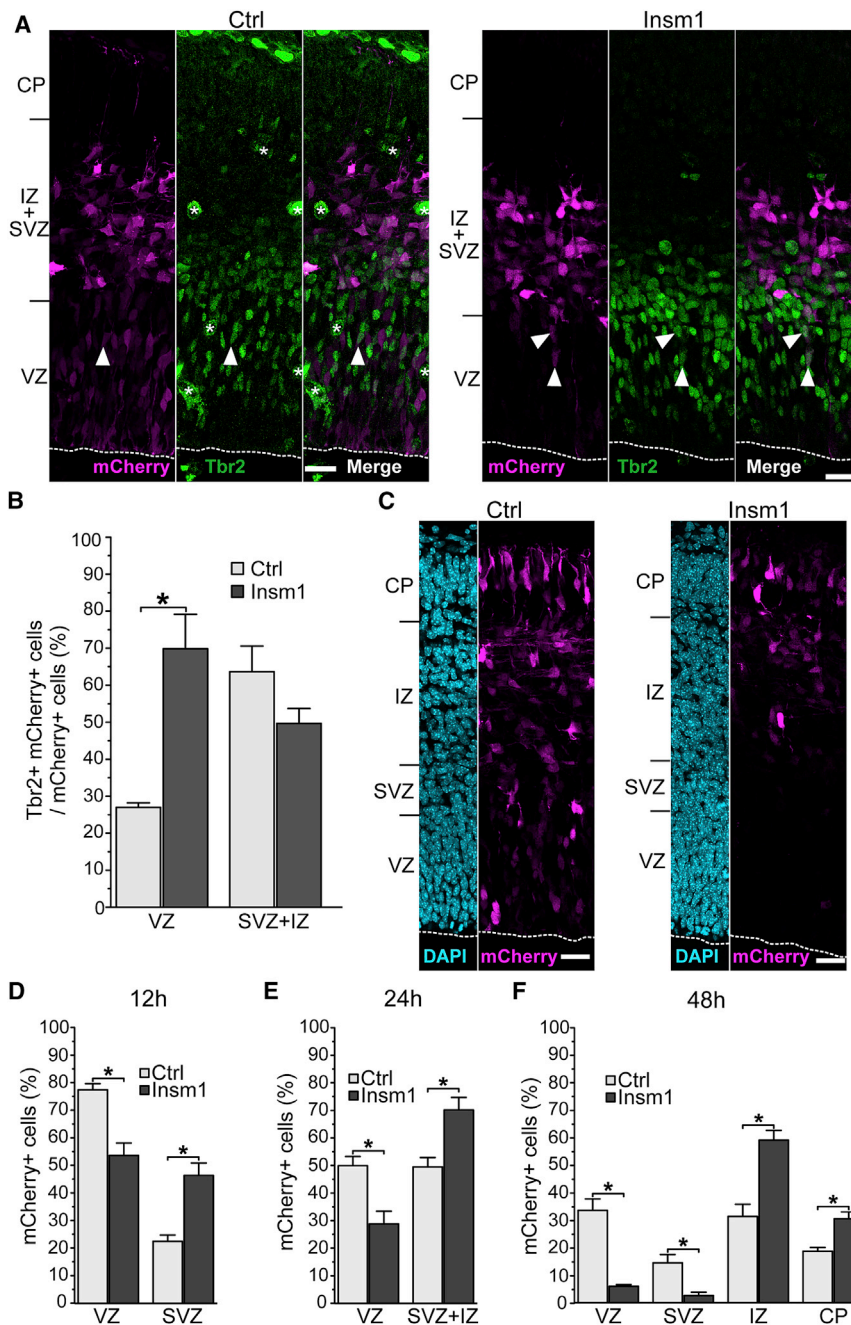


Figure 2. Insm1 FE in APs Increases the Generation of BPs

Mouse E12.5 Ncx was subjected to IUE with either an mCherry-encoding plasmid (Ctrl) or an Insm1-plus mCherry-encoding plasmid (Insm1), followed by analysis 12 (D), 24 (A, B, and E), or 48 (C and F) hr later. See also Figure S3A.

(A) mCherry (magenta) and Tbr2 (green) double IF upon Ctrl (left) and Insm1 (right) IUE. Arrowheads, mCherry⁺ Tbr2⁺ cells. Asterisks, autofluorescent blood vessels.

(B) The percentage of the mCherry⁺ cells in the VZ and SVZ+IZ that are Tbr2⁺ upon Ctrl (light gray) and Insm1 (dark gray) IUE.

(C) mCherry IF (magenta) and DAPI staining (cyan) upon Ctrl (left) and Insm1 (right) IUE.

(D–F) Distribution of the mCherry⁺ cells between the indicated Ncx zones, expressed as percentage of total, 12 (D), 24 (E) and 48 (F) hr after Ctrl (light gray) and Insm1 (dark gray) IUE. See also Figure S3B.

In (A) and (C), all images are maximum intensity projections (MIPs) of stacks of three 1- μ m optical sections (Z step size, 1.3 μ m). Dashed lines, VS. Scale bars, 25 μ m. In (B) and (D)–(F), data are the mean of 4 independent experiments with 1 littermate embryo each per experiment; error bars, SEM. * $p < 0.05$ (Mann-Whitney U test).

We first examined the expression of Tbr2 in the AP progeny (Figure 2A). Analysis 24 hr after IUE revealed that Insm1 FE more than doubled the proportion of Tbr2⁺ mCherry⁺ cells in the VZ, without increasing such cells in the SVZ (Figure 2B). In line with the increasingly generated Tbr2⁺ cells being newborn BPs, Insm1 FE massively shifted the progeny of the targeted APs that underwent mitosis to an abventricular location (Figures S3C–S3E).

We then analyzed the location, along the radial axis of the cortical wall, of the E12.5 targeted APs and their progeny at 12, 24, and 48 hr after IUE. Already at 12 hr after IUE, Insm1 FE decreased the proportion of mCherry⁺ cells in the VZ and increased that in the SVZ (Figure 2D).

The same was the case 24 hr after IUE, with a substantial proportion of the mCherry⁺ cells at a basal location now being in the intermediate zone (IZ) (Figures 2A and 2E). At 48 hr after IUE, Insm1 FE had caused a decrease in the proportion of targeted AP progeny in both VZ and SVZ and a corresponding increase in the IZ and CP (Figures 2C and 2F). The overwhelming majority ($\approx 80\%$) of the mCherry⁺ cells in the IZ, and almost all of the ones in the CP, were positive for the deep-layer neuron marker Tbr1 (Figure S3F). We conclude that Insm1 FE in APs either converts them to BPs or induces them to increasingly generate BPs, which in either case generate neurons.

expression (FE) of Insm1 at the onset of cortical neurogenesis promotes the premature generation of BPs (Farkas et al., 2008), one would expect that Insm1 FE in the course of neurogenesis increases the generation of BPs at the expense of AP abundance. To this end, we performed Insm1 FE by in utero electroporation (IUE) of APs in the E12.5 mouse Ncx, using a constitutive promoter and mCherry as a reporter to identify the progeny of the targeted APs (Figure S3A). Insm1 FE was readily detectable already 12 hr after IUE, with the Insm1 level being higher in the mCherry⁺ cells that had migrated to the SVZ than in those still located in the VZ (Figure S3B).

Insm1 FE in APs Causes NPC Delamination

If a primary function of Insm1 is exerted in the VZ, and, given that its FE results in either an AP-to-BP conversion or an increased BP generation from APs, one would expect Insm1 (1) to induce the delamination of NPCs from the VS, and (2) for Insm1 to be able to do so, to be endogenously expressed in NPCs still exhibiting apical contact. We first sought to investigate the latter point by examining the expression of the Insm1 protein in newborn BPs still attached to the VS. To this end, we made use of the transgenic mouse line *tg(Eomes::GFP)*, which expresses a cytosolic GFP under the control of the promoter of *Eomes*, which encodes the Tbr2 protein. As reported previously (Taverna et al., 2016), *Eomes::GFP*⁺ newborn BPs in the VZ can be found still attached to the VS (for an example, see Figure 3A). We then checked for the expression of Insm1 and Tbr2 in these newborn BPs (Figure 3B) and found that both transcription factors are indeed expressed. We conclude that the Insm1 protein is expressed in newborn BPs prior to their delamination.

We next investigated whether Insm1 induces delamination, using two complementary approaches, (1) Insm1 FE by IUE of E12.5 mouse *Ncx* and (2) microinjection (μ Inj) of *in-vitro*-transcribed *Insm1* mRNA into APs in organotypic slice culture of E13.5 mouse *Ncx*, a powerful method to dissect the behavior of single APs and their progeny (Taverna et al., 2011). As a first indicator of an increase in delamination, we performed IF for γ -tubulin (Figure 3C) and quantified the number of adventricular centrosomes within the VZ 12 hr after Insm1 IUE, i.e., at the earliest time point at which we have investigated the effects of Insm1 FE (see Figure 2D and Figure S3B). Insm1 FE increased adventricular centrosomes in the VZ 1.7-fold (Figure 3D). The magnitude of this increase was fully consistent with both, (1) the proportion of VZ NPCs that are newborn BPs in the control (Ctrl) condition (Figure 1B), and (2) the typically observed efficiency of AP targeting by IUE.

Next, we sought to directly determine whether Insm1 FE causes NPCs to lose their apical contact, that is, to retract from the VS and apical AJ belt. To this end, we microinjected *in-vitro*-transcribed mRNA for mRFP without, or together with, that for Insm1 into single APs of E13.5 mouse *Ncx*, and analyzed the morphology of cells as outlined by mRFP 24 hr later (Figure 3E). The presence or absence of apical contact of the RFP⁺ cells was corroborated by examining the position of the centrosome as revealed by γ -tubulin IF. *Insm1* mRNA μ Inj nearly doubled the proportion of RFP⁺ cells that lacked apical contact (Figure 3F). Moreover, in more than half of the cases, the RFP⁺ cells could be detected as pairs, suggesting that they were the daughter cells of a single microinjected AP (Figure 3E). In the Ctrl, more than two-thirds of the daughter cell pairs analyzed retained apical contact (Figure 3G). In contrast, upon *Insm1* mRNA μ Inj, for \approx 50% of the daughter cell pairs analyzed, both sibling cells had lost apical contact (Figure 3G). These data show that Insm1 causes NPC delamination from the VS.

Insm1 FE Promotes Delamination of aRG and Their Conversion to bRG

We then analyzed the morphology of the RFP⁺ cells that delaminated upon *Insm1* mRNA μ Inj. Interestingly, we found that almost

half of them (47%) exhibited a basal process, a morphological hallmark of bRG, with reflected a >2 -fold increase compared to the Ctrl (20%) (Figure 3H). To corroborate that these delaminated, basal process-bearing cells were bona fide bRG, we examined the expression of the bRG marker Sox2 (Figures 3I and 3J). Indeed, the vast majority of these cells (80%) were Sox2⁺ (Figure 3K). Taken together, these data indicate that the increase in NPC delamination caused by Insm1 FE includes an increase in bRG production.

This increased generation of bRG led us to hypothesize that, upon Insm1 FE, aRG lose their apical contact but not their basal process, resulting in an aRG-to-bRG transition. We used time-lapse live imaging to investigate this hypothesis and to analyze the details of the delamination process induced by Insm1 FE. To visualize the plasma membrane, we co-electroporated the E14.5 mouse *Ncx* with either Ctrl or Insm1-encoding plasmid along with a plasmid encoding GFP carrying the GAP43 membrane anchor under the control of a constitutive promoter. Observation of the morphology of delaminating cells during the time window of 10–35 hr after IUE revealed two principal cell types. First, cells that (1) did not show apically directed nuclear migration prior to the retraction of the plasma membrane from the VS (i.e., delamination), (2) exhibited an only short basal process, if any, prior to delamination, and (3) adopted a multipolar morphology after delamination, features characteristic of bIPs. Second, cells that (1) did show apically directed nuclear migration prior to delamination (provided that they could be observed sufficiently early), (2) exhibited a long basal process (extending beyond VZ and SVZ) prior to delamination, and (3) retained a radial morphology after delamination, features characteristic of radial glia.

In the Ctrl, almost all delaminating cells exhibited bIP morphology (Figures 4A and 4B; Movie S1). In contrast, upon Insm1 FE, 40% of the delaminating cells exhibited an aRG morphology before and a bRG morphology after delamination (Figures 4A and 4B; Movie S2). Of note, these delaminating cells retained a long basal process (Figure 4C). Considering the magnitude of delamination induced by Insm1 FE (Figures 3B and 3D), these data imply that most, if not all, of the cells that were induced to delaminate by the zinc finger transcription factor were aRG that were converted to bRG. Consistent with this, the vast majority of the latter cells underwent cell division at a basal location during the time of observation (Figure 4D). This increase in basal cell divisions was in line with the increase in basal mitoses observed 24 hr after Insm1 FE (Figures S3C and S3E). Taken together, these results demonstrate that Insm1 causes aRG to delaminate and convert into bRG.

Insm1 FE Represses AJ-Associated Components, Notably Plekha7

To gain insight at the molecular level about how Insm1 causes NPC delamination, we sought to identify potential Insm1 targets through a transcriptome analysis. Specifically, upon Insm1 FE in the developing mouse *Ncx* by IUE at E13.5, we isolated mCherry⁺ cells after 24 hr using fluorescence-activated cell sorting (FACS) and analyzed them by RNA sequencing (RNA-seq). Compared to the Ctrl, 640 genes were found to be differentially expressed (adjusted p value <0.05) in Insm1-targeted cells

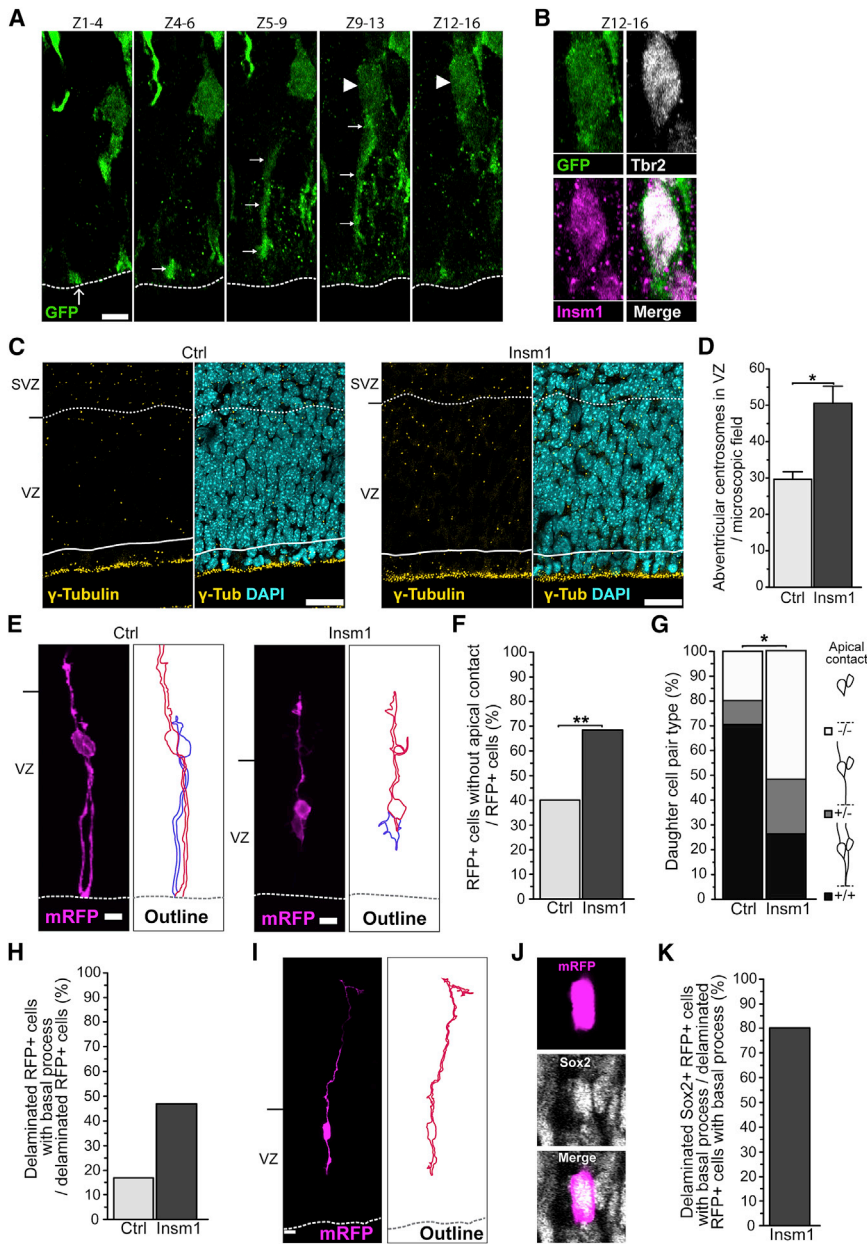


Figure 3. *Insm1* FE in APs Causes NPC Delamination

(A and B) Sequential MIP images showing z stacks comprising the indicated optical sections of a GFP-expressing nascent BP with apical attachment, in E14.5 *Ncx* of *Eomes::GFP* mouse.

(A) GFP IF (green). Large arrow, ventricular contact of the apical endfoot, small arrows, apical process; solid arrowheads, cell body.

(B) GFP (green), Tbr2 (white) and *Insm1* (magenta) triple IF of cell body shown in (A) (Z12–16).

(C and D) Mouse E12.5 *Ncx* was subjected to IUE with either an mCherry-encoding plasmid (Ctrl) or an *Insm1*- plus mCherry-encoding plasmid (*Insm1*), followed by analysis 12 hr later. See also Figure S3A.

(C) γ -tubulin (γ -Tub) IF (yellow) of electroporated area (identified by mCherry IF, not shown) upon Ctrl (left panels) and *Insm1* (right panels) IUE, without (left images of Ctrl and *Insm1*) and combined with (right images of Ctrl and *Insm1*) DAPI staining (cyan). Centrosomes (as revealed by γ -tubulin IF) in the VZ were defined as adventricular when located at least 15 μ m basal to the VS, with this distance being indicated by the solid lines. Dotted lines, boundary between VZ and SVZ.

(D) Adventricular centrosomes in the VZ (100- μ m-wide microscopic field) upon Ctrl (light gray) and *Insm1* (dark gray) IUE.

(E–K) *In-vitro*-transcribed *mRFP* mRNA either without (Ctrl) or together with (*Insm1*) *in-vitro*-transcribed *Insm1* mRNA was microinjected into single APs in organotypic slice culture of mouse E13.5 *Ncx*, followed by analysis 24 hr later.

(E) Examples of daughter cell pairs originating from single targeted APs upon Ctrl (left panels) and *Insm1* (right panels) mRNA μ lnj. Left images of Ctrl and *Insm1* show mRFP IF (magenta); right images show the cell outline as traced from that fluorescence. Cells exhibiting a basal process are outlined in magenta; cells lacking a basal process in the images shown are outlined in purple. Note that upon Ctrl mRNA μ lnj both daughter cells retain apical contact, whereas upon *Insm1* mRNA μ lnj both daughter cells have delaminated from the VS (indicated by the dashed lines).

(F) The percentage of mRFP⁺ cells that have lost apical contact upon Ctrl (light gray) and *Insm1* (dark gray) mRNA μ lnj (Ctrl, 12 mRFP⁺ cells analyzed in total; *Insm1*, 91 mRFP⁺ cells analyzed in total).

(G) The percentage of mRFP⁺ daughter cell pair types with regard to apical contact retention by both (+/+, black), only one (+/–, gray), or none (–/–, white) of the sibling cells, upon Ctrl (left, 10 cell pairs) and *Insm1* (right, 27 cell pairs) mRNA μ lnj.

(H) The percentage of delaminated mRFP⁺ cells that exhibit a basal process, upon Ctrl (light gray) and *Insm1* (dark gray) mRNA μ lnj (Ctrl, 12 mRFP⁺ cells analyzed in total; *Insm1*, 38 mRFP⁺ cells analyzed in total).

(I) Example of a delaminated mRFP⁺ cell exhibiting a basal process, upon *Insm1* mRNA μ lnj. Left image shows mRFP IF (magenta); right image shows the cell outline as traced from that fluorescence. Dashed lines, VS.

(J) mRFP (magenta) and Sox2 (white) double IF of delaminated cell body shown in (I).

(K) The percentage of delaminated mRFP⁺ cells with a basal process that are Sox2⁺, upon *Insm1* mRNA μ lnj (10 cells analyzed in total).

Images in (A)–(C), (E), and (I) are MIPs of 3–5 (A), 5 (B), 3 (C), 38 (E, Ctrl), 54 (E, *Insm1*), and 104 (I) optical sections; image in (H) is a single optical section. Optical section thickness and Z step-size are 1 and 0.8 μ m, respectively, in (A) and (B), 1 and 1.3 μ m, respectively, in (C), and 0.8 and 0.6 μ m, respectively, in (E), (I), and (J). Scale bars, 5 μ m in (A), 25 μ m in (C), and 10 μ m in (E) and (I).

Data in (D) are the mean of 4 independent experiments with 1 littermate embryo each per experiment; error bars, SEM. Data in (F–H) and (K) are pooled from 6 (F–H) or 3 (K) independent experiments with 1 embryo per experiment. * $p < 0.05$; ** $p < 0.01$ (Mann-Whitney U test in D, Fisher's exact test in F, and chi-square test in G).

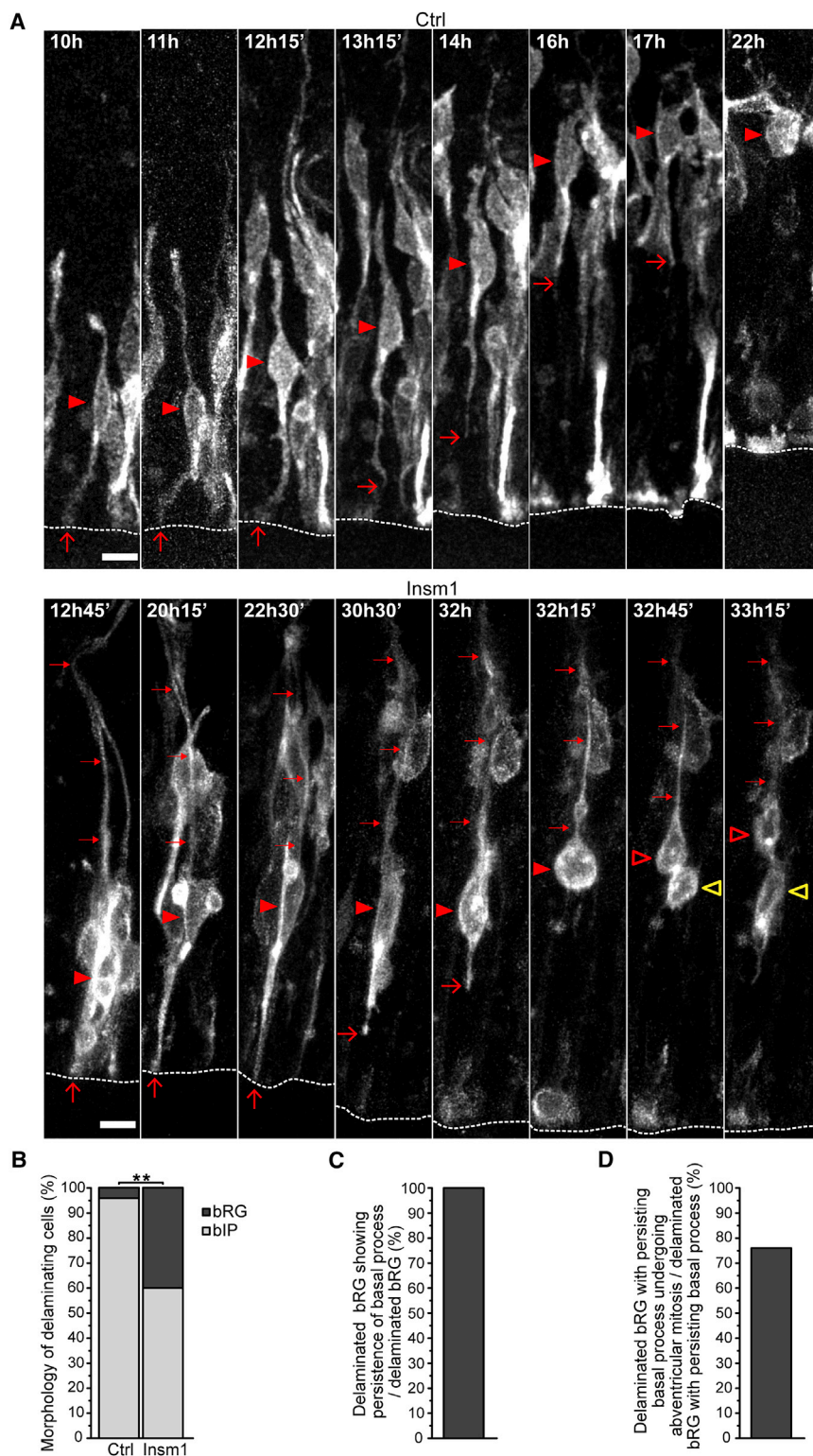


Figure 4. Insm1 FE Converts aRG to Delaminated bRG

Mouse E14.5 Ncx was subjected to IUE with a membrane-GFP-encoding plasmid plus either an mCherry-encoding plasmid (Ctrl) or an Insm1- plus mCherry-encoding plasmid (Insm1), followed by time-lapse live imaging (time range 10–35 hr after IUE) and analysis. See also Figure S3A.

(A) Still images of cells exhibiting membrane-GFP fluorescence upon Ctrl (top row) and Insm1 (bottom row) IUE. Time after IUE is indicated at the top of each image. Top row shows a delaminating bIP; arrowheads, cell body; arrows, ventricular contact of the apical endfoot (until 12 hr 15 min) and apical-most position of the retracting apical process. See also Movie S1. Bottom row shows an aRG and its conversion to a delaminated bRG; solid arrowheads, cell body of the delaminating NPC; open arrowheads, cell bodies of the two daughter cells arising therefrom; large arrows, ventricular contact of apical endfoot (until 22 hr 30 min), and apical-most position of retracting apical process; small arrows, basal process. See also Movie S2. All images are MIPs of 17–38 optical sections (1 μ m; Z step-size, 0.8 μ m). Dashed lines, VS. Scale bars, 10 μ m.

(B) The percentage of delaminating membrane-GFP⁺ cells that exhibit either bIP morphology (light gray) or bRG morphology (dark gray) upon Ctrl (left, 21 cells) and Insm1 (right, 55 cells) IUE. Data are from 3 independent experiments with 1 littermate embryo each per experiment. ***p* < 0.01 (Fisher's exact test).

(C) The percentage of the 22 delaminating bRG upon Insm1 IUE (see B) that after delamination show persistence of the basal process during the subsequent time of live imaging.

(D) The percentage of the 22 delaminating bRG upon Insm1 IUE (see B), all of which after delamination show persistence of the basal process (see C), that undergo abventricular mitosis during the time of live imaging.

expression compared to Ctrl (406 genes, collectively referred to as Insm1-downregulated genes), and less than one-third showed an increased expression (234 genes, collectively referred to as Insm1-upregulated genes).

Gene ontology (GO) terms enrichment analysis followed by a functional annotation clustering analysis of the differentially expressed genes revealed that for the GO term category biological process, the top five GO term clusters were related to cell/neuron morphogenesis, cell adhesion, regulation of neurogenesis, forebrain development, and cell migration (Figure 5B; Table S1). These GO term clusters were consistent with specific biological processes that are known to be involved in NPC delamination and would therefore be expected to be

(Figure 5A; Table S1). In line with the transcriptional repressor activity of Insm1 as a member of the SNAG family zinc finger transcription factors (Chiang and Ayyanathan, 2013), the majority of the differentially expressed genes showed a decreased

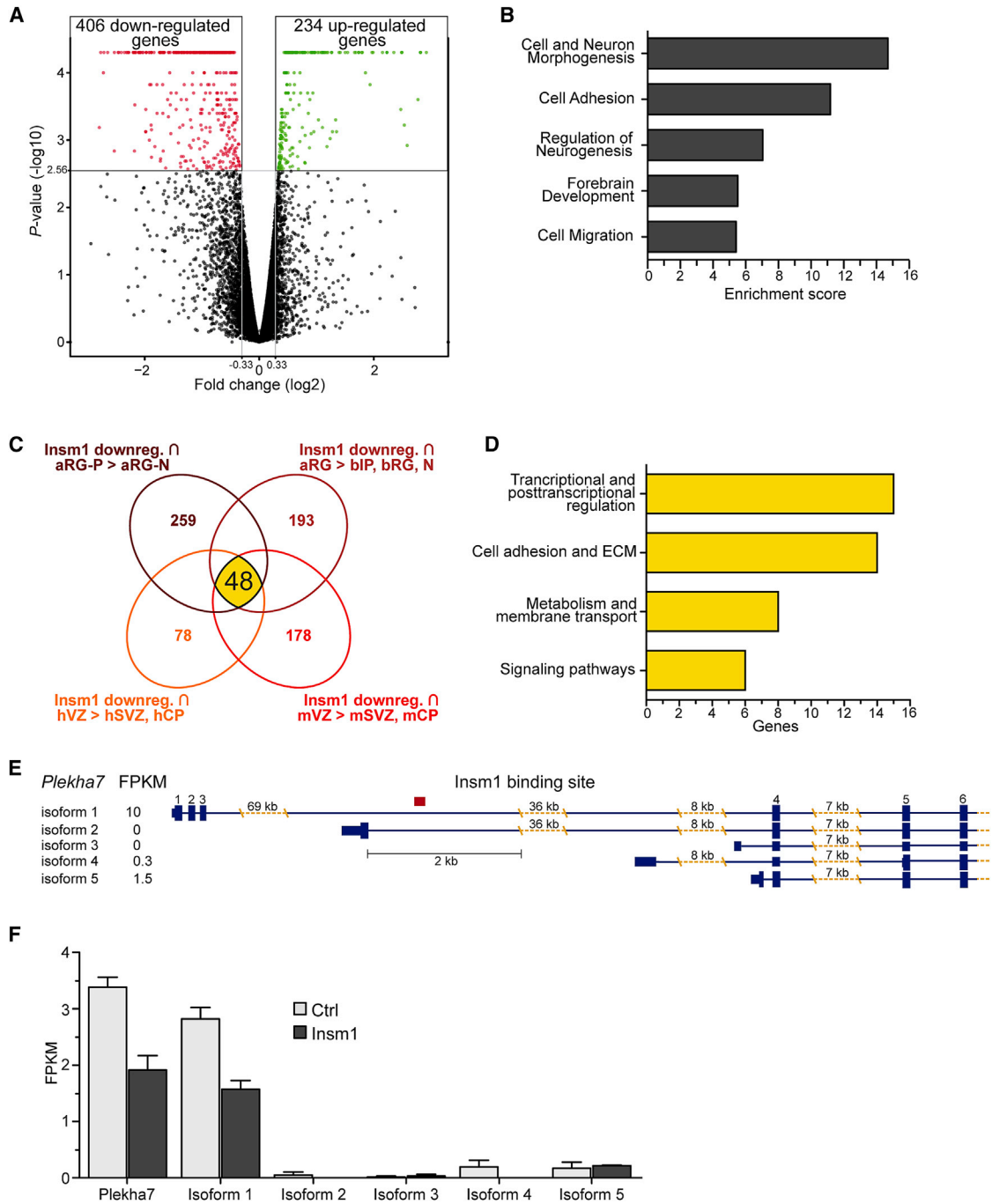


Figure 5. Insm1 FE Represses *Plekha7*

(A–D and F) Mouse E13.5 Ncx was subjected to IUE with either an mCherry-encoding plasmid (Ctrl) or an Insm1- plus mCherry-encoding plasmid (Insm1), followed 24 hr later by isolation of mCherry⁺ cells using FACS and by RNA-seq. See also Figure S3A.

(A) Volcano plot showing the changes in gene expression upon Insm1 IUE compared to Ctrl. Red dots, downregulated genes; green dots, upregulated genes; black dots, genes without a significant change in expression level (adjusted $p < 0.05$, corresponding to p value $> -\log_{10}(2.56)$ [horizontal line]). See also Figure S7 and Table S1.

(B) Top five clusters of enriched GO terms in the category biological process associated with the Insm1 differentially expressed genes. See also Table S1.

(C) Venn diagram showing the numbers of the 406 Insm1-downregulated genes (Insm1 downreg.) that in previous transcriptome datasets have been found to be more highly expressed in mouse proliferative aRG than neurogenic aRG (aRG-p > aRG-N; top left) (Florio et al., 2015), in mouse aRG than bIPs, bRG, and neurons

(legend continued on next page)

affected by *Insm1*, that is, (1) changes in NPC morphology, (2) loss of apical cell adhesion, (3) production neurogenic NPCs, and (4) migration to the SVZ.

To further home in on potential *Insm1* targets involved in NPC delamination, we concentrated on the 406 *Insm1*-downregulated genes, given that *Insm1* is a transcriptional repressor (Chiang and Ayyanathan, 2013). To this end, we asked which of these genes would show changes in expression levels in previously published transcriptome datasets (Fietz et al., 2012; Florio et al., 2015) in line with the process of NPC delamination. Specifically, we extracted four groups of genes exhibiting such changes in expression, genes more highly expressed in (1) mouse proliferative aRG than neurogenic aRG, (2) mouse aRG than bIPs, bRG, and neurons, (3) mouse VZ than SVZ and CP, and (4) human VZ than SVZ and CP. Of the 259, 193, 178, and 78 *Insm1*-downregulated genes in groups i–iv, respectively (Figure S4), 48 were common to all four groups (Figure 5C; Table S2).

We then analyzed these 48 genes with regard to the functions exerted by the respective proteins. This revealed two major functional groups, (1) proteins involved in transcriptional and post-transcriptional regulation (15 members, Figure 5D; Table S2), and (2) proteins with roles related to extracellular matrix (ECM) and cell adhesion (14 members, Figure 5D; Table S2), followed by (3) proteins with functions in metabolism and membrane transport (8 members, Figure 5D; Table S2), and (4) proteins involved in signaling pathways (notch, growth factors) (6 members, Figure 5D; Table S2). As the functional groups 1, 3, and 4 encompass a wide variety of cellular processes, but our goal was to obtain mechanistic insight into the *Insm1*-induced delamination process, we analyzed the known features of the 14 proteins in group 2 (ECM and cell adhesion) for a potential role in this process.

A major step in the delamination process is the disengagement of the delaminating cells from the apical AJ belt (Wilsch-Bräuninger et al., 2016). Only two of the 14 proteins in group 2 are known to exert roles related to AJs – Ajuba and *Plekha7*. Ajuba is a LIM domain-containing protein shown to interact with α -catenin and to play a role in AJ establishment and stability (Marie et al., 2003; Nola et al., 2011). However, Ajuba also exerts roles in a variety of other cellular processes that are not directly related to AJs and delamination, e.g., microRNA-mediated gene silencing (James et al., 2010). We therefore concentrated our efforts on *Plekha7*, for which the available evidence clearly indicates that its major role is primarily related to AJs (Shah et al., 2016).

Studies in systems other than the developing brain have established that *Plekha7* interacts with two major components of AJs, (1) afadin, which links the transmembrane proteins nectins to the actin cytoskeleton, and (2) p120-catenin, thereby

providing a link between the transmembrane proteins cadherins and the microtubule system (Shah et al., 2016) (Figures S5A and S5B). Moreover, *Plekha7* overexpression and knockdown in epithelial cell cultures have been shown to affect the integrity of AJs (Meng et al., 2008). In light of these data, we asked whether the downregulation of the *Plekha7* mRNA level upon *Insm1* FE in embryonic mouse *Ncx* (Table S2) could reflect a direct repressive action of *Insm1* on the *Plekha7* gene. Indeed, using a recently published *Insm1* chromatin immunoprecipitation sequencing (ChIP-seq) dataset (Jia et al., 2015), we identified an *Insm1* binding site located ≈ 71 kb 3' from the 5' beginning of the large, ≈ 118 kb intron 3 of the *Plekha7* isoform 1 (Figure 5E). Previous transcriptome data (Fietz et al., 2012) indicate that, of the five *Plekha7* isoforms described to date (O'Leary et al., 2016), isoform 1 shows by far the highest mRNA expression level in mouse E14.5 VZ (Figure 5E). The present transcriptome analysis of the Ctrl and *Insm1*-targeted cells corroborated these data and showed that by far the greatest decrease in *Plekha7* mRNA FPKM values upon *Insm1* FE was found for isoform 1 (Figure 5F).

***Plekha7* Is Specifically Associated with Apical AJs in the Mouse Embryonic VZ**

We therefore investigated whether, in embryonic mouse *Ncx*, *Plekha7* is associated with the apical AJs, and whether *Insm1* FE reduces its level. Double IF of the mouse E14.5 *Ncx* indicated that *Plekha7* was confined to the apical-most region of the *Ncx* (Figure 6A). Specifically, *Plekha7* IF overlapped with the apical-most IF for cadherin and p120-catenin and also coincided with the apical F-actin cytoskeleton as revealed by phalloidin staining but was absent from the apical domain proper lacking cadherin IF (Figures 6B, S5C, and S5D). Immunogold electron microscopy of the apical region of the mouse E14.5 VZ showed that *Plekha7* was concentrated over apical AJs (Figures 6C–6E). Taken together, these results demonstrate that, in the mouse developing *Ncx*, *Plekha7* is specifically associated with the apical AJ belt.

Being able to detect the presence of *Plekha7* in association with apical AJs, we sought to verify that the reduction in the *Plekha7* mRNA level observed upon *Insm1* FE in the mouse embryonic *Ncx* (Figure 5F; Table S2) actually resulted in a decrease in AJ-associated *Plekha7* protein. We therefore measured the *Plekha7* IF at the AJs of mCherry⁺ APs 24 hr after Ctrl and *Insm1* IUE. Similar to the observations shown in Figure 2, upon *Insm1* FE, fewer mCherry⁺ cells were found to be still attached at the ventricle than in the Ctrl, in line with the delamination-inducing function of *Insm1* (Figures 2 and 3). In these *Insm1*-targeted, still apically attached NPCs, *Plekha7* IF at the AJs was significantly decreased as compared to apically

(aRG > bIP, bRG, N; top right) (Florio et al., 2015), in mouse VZ than SVZ and CP (mVZ > mSVZ, mCP; bottom right) (Fietz et al., 2012), and in human VZ than SVZ and CP (hVZ > hSVZ, hCP; bottom left) (Fietz et al., 2012), and the number of genes common to these four groups. See also Figure S4.

(D) Major functional groups of the proteins encoded by the 48 genes common to the four groups shown in (C). See also Table S2.

(E) Genomic organization of the five *Plekha7* isoforms (RefSeqs) until exon 6 of isoform 1, and their expression level (FPKM) in the mouse VZ (Fietz et al., 2012). Exons, blue boxes; introns, blue lines. Location of the identified *Insm1* binding site in intron 3 of isoform 1 (Jia et al., 2015) is indicated by the red box.

(F) Total *Plekha7* mRNA (*Plekha7*) and *Plekha7* isoform mRNA expression levels (FPKM) upon Ctrl (light gray) and *Insm1* (dark gray) IUE.

In (A) and (F), data are the mean of 3 independent experiments, with 2 littermate embryos each per experiment being pooled for isolation of mCherry⁺ cells using FACS followed by RNA-seq; error bars in (F), SEM.

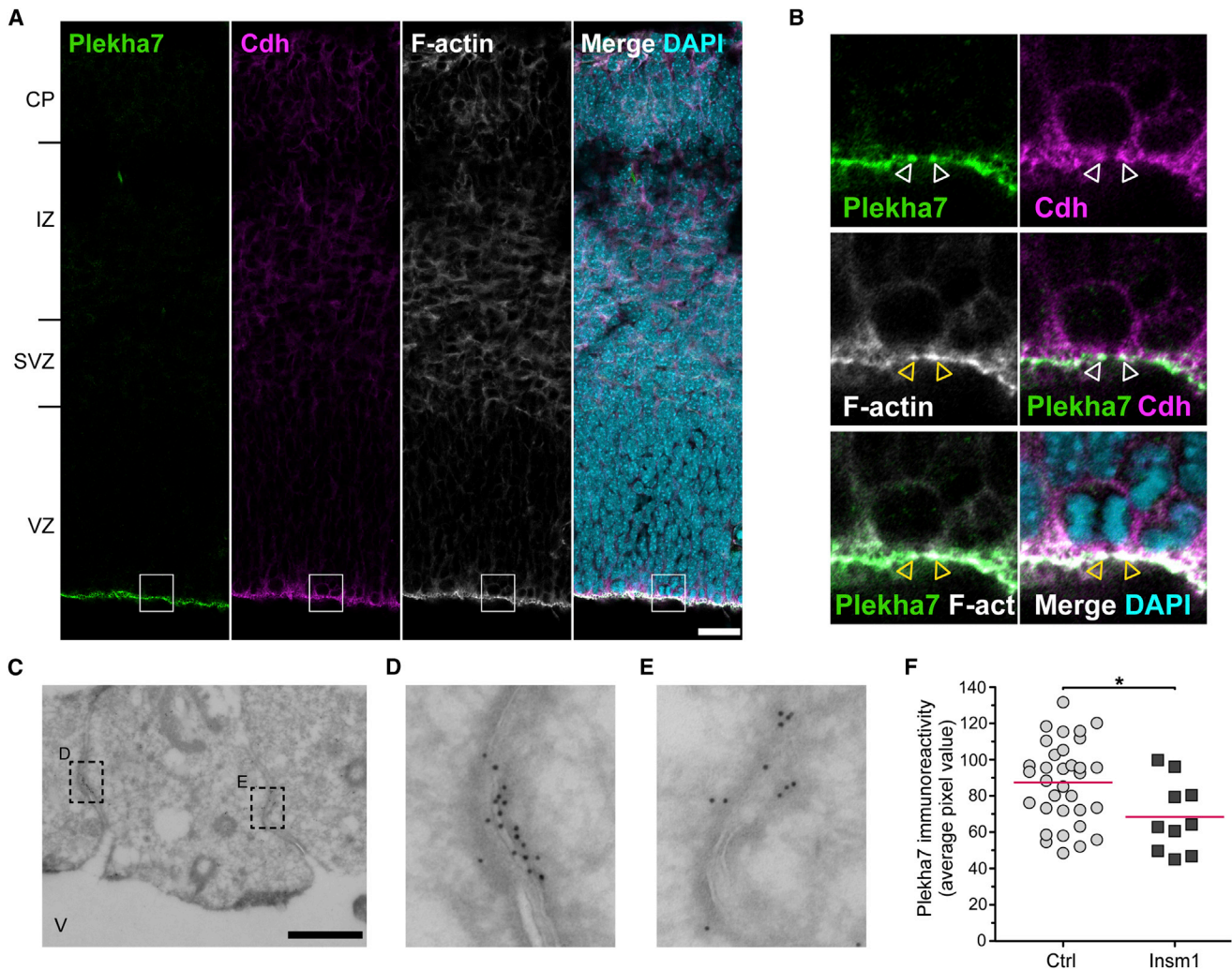


Figure 6. Plekha7 in Mouse Embryonic Ncx Is Concentrated at the Apical AJ Belt

(A and B) Plekha7 (green) and cadherin (magenta) double IF, F-actin (F-act) staining using fluorescently labeled phalloidin (white), and DAPI staining (cyan) of E14.5 mouse Ncx. Images are single 1- μ m optical sections. See also [Figures S5A–S5C](#).

(A) Overview of Ncx. Boxes indicate region shown at higher magnification in (B). Scale bar, 25 μ m.

(B) Higher magnification of the apical region of the VZ. Note the co-localization of Plekha7 IF with the apical-most cadherin IF, indicative of the concentration of Plekha7 at AJs (arrowheads).

(C–E) Transmission electron micrographs of apical region of VZ of E14.5 mouse Ncx showing the localization of Plekha7 at the apical AJ belt by immunogold labeling. Dashed boxes in (C) indicate regions shown at higher magnification in (D) and (E). V, ventricle. Scale bar, 2 μ m.

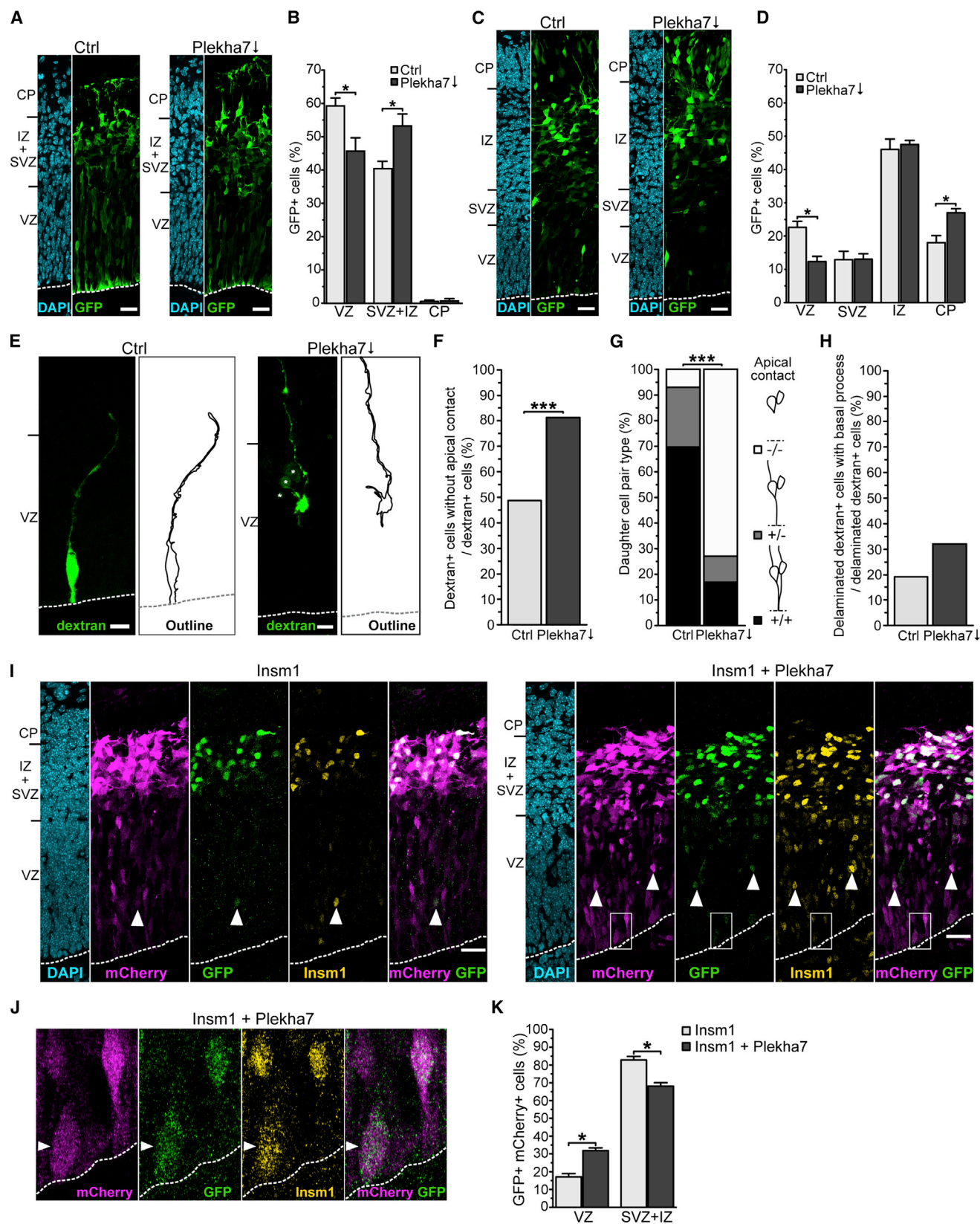
(F) Mouse E12.5 Ncx was subjected to IUE with either an mCherry-encoding plasmid (Ctrl) or an Insm1- plus mCherry-encoding plasmid (Insm1) (see [Figure S3A](#)), followed by analysis of Plekha7 IF 24 hr later. Individual data points show quantification of Plekha7 IF (average pixel value) at the apical AJs of mCherry⁺ cells upon Ctrl (light gray circles, 33 cells) and Insm1 (dark gray squares, 10 cells) IUE; red lines, mean. * $p < 0.05$ (unpaired Student's t test).

attached Ctrl NPCs ([Figure 6F](#)). These data show that Insm1 FE, most likely via direct repression of *Plekha7* transcription, results in a reduction in the amount of Plekha7 protein that is associated with the AJ belt.

Disruption of *Plekha7* Expression Causes NPC Delamination

To directly determine whether decreasing the AJ-associated Plekha7 protein results in NPC delamination, we used the CRISPR/Cas9 technology to disrupt expression of the *Plekha7* gene in APs. Our lab recently developed a procedure ([Kalebic](#)

[et al., 2016](#)) to disrupt the expression of genes of interest in APs and their progeny, by applying the CRISPR/Cas9 technology together with established approaches to manipulate gene expression in the developing Ncx, that is, IUE and μ Inj into APs in organotypic slice culture ([Taverna et al., 2011](#)). To disrupt *Plekha7* expression, we designed five guide RNAs (gRNAs) targeting either exon 5 or exon 6 of *Plekha7* isoform1 ([Figure S6A](#)), two exons common to all 5 *Plekha7* isoforms ([Figure 5E](#)). In an *in vitro* assay, two of these gRNAs, gRNA4 and gRNA5, in combination with recombinant Cas9 protein resulted in nearly complete cutting of exon 6 and exon 5 DNA, respectively, using a



(legend on next page)

1.2-kb PCR-amplified template (Figure S6B). To examine whether this approach would result in disruption of *Plekha7* expression in intact epithelial cells, we co-transfected Eph4-Ev cells, a mouse mammary epithelial cell line, with either a plasmid encoding Cas9 and a gRNA against the *LacZ* gene (Kalebic et al., 2016) plus a plasmid encoding GFP (Ctrl), or a plasmid encoding Cas9 and gRNA4 and gRNA5 plus a plasmid encoding GFP (disruption), followed by replating of cells after 1 day and analysis after a further 3 days. As shown in Figures S6C–S6E, this resulted in a massive reduction in *Plekha7* IF at the apical AJ formed by these cells in culture.

We therefore introduced a mixture of gRNA4 and gRNA5, each complexed with recombinant Cas9 protein, together with a GFP-encoding plasmid into APs by IUE at E12.5, and analyzed the distribution of GFP⁺ cells across the cortical wall, notably the germinal zones, 24 hr later (Figure 7A). (IUE of recombinant Cas9 protein has been shown to cause disruption of gene expression within 24 hr that is at least as efficient as that obtained with IUE of a Cas9-encoding plasmid; Kalebic et al., 2016.) As Ctrl, we used a previously published gRNA against the *LacZ* gene (Kalebic et al., 2016). This approach of disrupting *Plekha7* expression resulted in a significant decrease in the percentage of the progeny of the targeted APs found in the VZ and in a concomitant increase in the AP progeny in the SVZ/IZ (Figures 7A and 7B). To further study the fate of the latter AP progeny, we performed IUE of E12.5 mice using a plasmid encoding Cas9, gRNA4, and gRNA5, as well as a GFP, and quantified the distribution of GFP⁺ cells between the germinal zones and the CP at E14.5. At this later

time point of analysis, the decrease in the AP progeny found in the VZ had its counterpart in a corresponding increase in AP progeny in the CP (Figures 7C and 7D). We conclude that disrupting *Plekha7* expression promotes the delamination of NPCs, resulting in an increase in BPs and eventually in neurons in the CP.

This conclusion implies that disruption of *Plekha7* expression does not affect the NPC nature of the cells in the VZ and therefore does not induce direct neurogenesis. We sought to obtain evidence in support of this notion and therefore analyzed the expression of the NPC marker Pax6 and the neuronal marker Tuj1 in the VZ 24 hr after *Plekha7* gene disruption (Figures S6F–S6H). For both markers, we did not observe differences between Ctrl and *Plekha7* gene disruption (Figures S6G and S6H). Specifically, virtually all progeny of the targeted cells in the VZ (1) remained Pax6⁺ and (2) lacked Tuj1 expression, upon *Plekha7* gene disruption. Taken together these data show that the increase in cells residing in the CP 48 hr after *Plekha7* gene disruption (Figures 7C and 7D) is not due to direct neurogenesis, but rather to an increased generation of BP, which subsequently will give rise to neurons.

To further dissect, at the single AP level, the effect of disrupting *Plekha7* expression, we again made use of the μ lnj method (Taverna et al., 2011). Specifically, we introduced the same recombinant Cas9 protein/gRNA complexes as used for IUE (Figures 7A and 7B), together with fluorescently labeled dextran as a membrane-impermeable tracer, into single APs in organotypic slice culture of E13.5 mouse Ncx, and analyzed the morphology of the microinjected APs/their progeny as outlined

Figure 7. Disruption of *Plekha7* Expression Causes NPC Delamination from the VS

(A–D) Mouse E12.5 Ncx was subjected to IUE (1) with a GFP-encoding plasmid plus recombinant Cas9 protein complexed with either *LacZ* gRNA (Ctrl) or *Plekha7* gRNA4 and gRNA5 (*Plekha7* \downarrow) (A and B) or (2) with either a Cas9-, *LacZ* gRNA-, and GFP-encoding plasmid (Ctrl) or a Cas9-, gRNA4-, gRNA5-, and GFP-encoding plasmid (*Plekha7* \downarrow) (C and D), followed by analysis either 24 hr (A and B) or 48 hr (C and D) later. See also Figures S6A–S6E. (A and C) GFP IF (green) and DAPI staining (cyan) either 24 (A) or 48 (C) hr after Ctrl (left panels) and *Plekha7* \downarrow (right panels) IUE. (B and D) Distribution of GFP⁺ cells between the indicated Ncx zones, expressed as percentage of total, either 24 (B) or 48 (D) hr after Ctrl (light gray) and *Plekha7* \downarrow (dark gray) IUE.

(E–H) Recombinant Cas9 protein complexed with either *LacZ* gRNA (Ctrl) or *Plekha7* gRNA4 and gRNA5 (*Plekha7* \downarrow), together with fluorescently labeled dextran, was microinjected into single APs in organotypic slice culture of mouse E13.5 Ncx, followed by analysis 24 hr later. See also Figures S6A–S6E.

(E) Examples of targeted cells upon Ctrl (left panels) and *Plekha7* \downarrow (right panels) μ lnj. Left images of Ctrl and *Insm1* show dextran IF (green); right images show the cell outline as traced from that fluorescence. Note that the cell shown for the Ctrl μ lnj retains apical contact and exhibits a basal process, whereas the cell shown for *Plekha7* \downarrow μ lnj has delaminated from the VS (indicated by the dashed lines) but still exhibits a basal process.

(F) The percentage of dextran⁺ cells that have lost apical contact upon Ctrl (light gray) and *Plekha7* \downarrow (dark gray) μ lnj (Ctrl, 41 dextran⁺ cells analyzed in total; *Plekha7* \downarrow , 107 dextran⁺ cells analyzed in total).

(G) The percentage of dextran⁺ daughter cell pair types with regard to apical contact retention by both (+/+, black), only one (+/–, gray), or none (–/–, white) of the sibling cells upon Ctrl (left, 13 cell pairs) and *Plekha7* \downarrow (right, 29 cell pairs) μ lnj.

(H) The percentage of delaminated dextran⁺ cells that exhibit a basal process, upon Ctrl (light gray) and *Plekha7* \downarrow (dark gray) μ lnj (Ctrl, 26 delaminated dextran⁺ cells analyzed in total; *Plekha7* \downarrow , 99 delaminated dextran⁺ cells analyzed in total).

(I–K) Mouse E12.5 Ncx was subjected to IUE with an *Insm1*- plus nuclear GFP-encoding plasmid together with either an mCherry-encoding plasmid (*Insm1*) or a *Plekha7*- plus mCherry-encoding plasmid (*Insm1* + *Plekha7*) (see Figure S6J), followed by analysis 24 hr later.

(I) mCherry (magenta), GFP (green), and *Insm1* (yellow) triple IF and DAPI staining (cyan) upon *Insm1* (left) and *Insm1* + *Plekha7* (right) IUE. Arrowheads, mCherry⁺ GFP⁺ *Insm1*⁺ cells in the VZ. Boxes indicate region shown at higher magnification in (J).

(J) mCherry (magenta), GFP (green), and *Insm1* (yellow) triple IF of the boxed region in (I), showing a cell body (arrowheads) co-expressing *Insm1* and *Plekha7* (as revealed by mCherry IF) that is still attached to the VS 24 hr after *Insm1* + *Plekha7* IUE.

(K) Distribution of the GFP⁺ mCherry⁺ cells between the indicated Ncx zones, expressed as percentage of total, upon *Insm1* (light gray) and *Insm1* + *Plekha7* (dark gray) IUE.

All images are MIPs of 3 (A, C, I, and J), 19 (E, Ctrl), and 13 (E, *Plekha7* \downarrow) optical sections. Optical section thickness and Z step-size are 1 and 1.3 μ m, respectively, in (A), (C), (I), and (J), 0.8 and 0.6 μ m, respectively, in (E) (Ctrl), and 1 and 1 μ m, respectively, in (E) (*Plekha7* \downarrow). Dashed lines, VS. Asterisks, autofluorescent blood vessels. Scale bars, 25 (A, C, and I) and 10 (E) μ m.

Data in (B), (D), and (K) are the mean of 5 (B) and 4 (D and K) independent experiments with 1–2 littermate embryos each per experiment; error bars, SEM. Data in (F)–(H) are pooled from 7 (F and G) and 3 (H) independent experiments with 1 embryo each per experiment. **p* < 0.05; ****p* < 0.001 (Mann-Whitney U test in B, D, and K, Fisher's exact test in F, and chi-square test in G).

by dextran 24 hr later (Figure 7E). The presence or absence of apical contact of the dextran⁺ cells was corroborated by IF for γ -tubulin and Arl13b as markers of centrosome and primary cilium, respectively. Similar to the results obtained upon μ lnj of *Insm1* mRNA (Figure 3D), disruption of *Plekha7* expression by Cas9 protein/gRNA μ lnj doubled the proportion of dextran⁺ cells that lacked apical contact compared to Ctrl (Figure 7F). For both Ctrl and *Plekha7* disruption, more than half of the dextran⁺ cells analyzed could be detected as pairs of sibling cells. Analysis of these pairs revealed that, in the Ctrl, their vast majority consisted of two sibling cells that retained apical contact (Figure 7G). In contrast, upon disruption of *Plekha7* expression by Cas9 protein/gRNA μ lnj, the vast majority of these pairs consisted of two sibling cells, both of which had lost apical contact (Figure 7G).

Two additional observations complemented these data. First, the few dextran⁺ cells still exhibiting apical contact 24 hr after disruption of *Plekha7* expression by Cas9 protein/gRNA μ lnj showed an increase in the proportion of cells that were not only Sox2⁺, but also Tbr2⁺ (Figure S6I), consistent with *Plekha7* downregulation promoting BP generation. Second, this approach of disrupting *Plekha7* expression nearly doubled the percentage of delaminated dextran⁺ cells that retained a basal process (Figure 7H). Collectively, these data not only demonstrate that disruption of *Plekha7* expression causes NPC delamination from the VS, including the generation of bRG. They also imply that *Plekha7*, via its role at the apical AJ belt (Meng et al., 2008), is necessary for NPCs to maintain their apical contact.

***Plekha7* FE Increases the Retention of Cells in the VZ and Reverts the *Insm1*-Induced NPC Delamination**

Given these findings, we next asked whether an increase in the AJ belt-associated *Plekha7* level would impair NPC delamination. To this end, we performed *Plekha7* FE using plasmids expressing either *Plekha7* and mCherry or only mCherry under the control of a constitutive promoter (Figure S6K). Transfection of EpH4-Ev cells with the *Plekha7*-expressing plasmid showed that this resulted in an increase in *Plekha7* IF at apical AJs (Figure S6L). We then performed IUE with these plasmids at E12.5 and analyzed the proportion of mCherry⁺ cells remaining in the VZ after 48 hr (Figures S6M and S6N). Compared to Ctrl, a greater proportion of the mCherry⁺ cells was found to be located in the VZ upon *Plekha7* FE (Figure S6N). These data suggest that the intrinsic delamination process is impeded by increasing *Plekha7* levels at apical AJs.

In light of these data, we investigated whether *Plekha7* FE along with *Insm1* would suffice to revert the *Insm1*-induced NPC delamination. To this end, we generated a plasmid encoding *Insm1* and nuclear GFP to be used for co-expression with either *Plekha7* plus mCherry, or only mCherry as Ctrl (Figure S6J). IUE of these plasmids into the E12.5 mouse Ncx, followed by analysis of the distribution of the GFP⁺ mCherry⁺ cells across the cortical wall 24 hr later (Figure 7I), revealed that *Plekha7* co-expression with *Insm1* doubled the proportion of the progeny of the targeted cells that remained in the VZ (Figure 7K), with *Insm1*⁺ *Plekha7*⁺ cells remaining attached to the VS (for an example, see Figure 7J). We conclude that increasing *Plekha7*

levels at apical AJs can suffice to revert the *Insm1*-induced NPC delamination.

DISCUSSION

Downregulation of the AJ Belt-Specific Protein *Plekha7* Causes BP Delamination in the Developing Ncx

We have identified a novel target to induce BP delamination in the developing Ncx—the AJ belt-specific protein *Plekha7*. BP delamination in the context of cortical neurogenesis occurs after APs, the primary source of BPs, have lost their tight junctions (Wilsch-Bräuninger et al., 2016). Therefore, components of the AJ belt constitute prime targets to be subject to downregulation and thereby to induce BP delamination. Compared to other AJ components implicated in NPC delamination (Wilsch-Bräuninger et al., 2016), four features render *Plekha7* a unique target to induce this process. First, of all AJ components examined, *Plekha7* is the major target of downregulation by *Insm1*, a transcription factor with a panneurogenic role that has been shown to promote BP generation (Farkas et al., 2008). Second, *Plekha7* has a particularly strategic location within the complex structure of the AJ belt of NPCs, being associated with both the cadherin and the nectin system, and hence the two principal transmembrane protein-to-cytoskeleton assemblies of the AJ belt (Shah et al., 2016). Third, in contrast to these major AJ components, which are found not only on the apical AJ belt but also on more basally located spot-like AJ (Hirano and Takeichi, 2012; Rikitake et al., 2012; Wilsch-Bräuninger et al., 2016), *Plekha7* is only associated with the apical AJ belt (Shah et al., 2016), as is further discussed below. Fourth, *Plekha7*, via its interaction with Nezha/CAMSAP3, links the microtubule-based cytoskeleton to the AJ belt (Meng et al., 2008). Given these features, a reduction in *Plekha7* levels in APs might therefore cause NPC delamination. Indeed, CRISPR/Cas9-mediated disruption of *Plekha7* expression in APs of mouse embryonic Ncx resulted in a marked increase in delamination of NPC, including bRG.

Although the details of the underlying mechanism how disruption of *Plekha7* expression leads to NPC delamination remains to be investigated, observations in non-neural epithelial cells provide some clues. Thus, *Plekha7* has been found to be required for the integrity of the AJ belt in epithelial monolayers formed by various cell lines *in vitro* (Shah et al., 2016). Specifically, the interaction of Nezha-capped microtubules with *Plekha7* has a key role in the recruitment of the minus-end motor protein Kifc3 to the AJ belt. Kifc3 binds the ubiquitin-specific protease Usp47 and promotes its localization at the AJ belt. Usp47 in turn inhibits the proteolytic degradation of E-cadherin by deubiquitinating their cytoplasmic domain (Sako-Kubota et al., 2014). Accordingly, the knockdown of *Plekha7*, presumably by interfering with this cascade of events, results in the reduction of E-cadherin levels at the AJ belt (Meng et al., 2008). Extrapolating from these findings, disruption of *Plekha7* expression in APs may impair the integrity of the AJ belt, thereby promoting NPC delamination.

In this context, it is important to realize a unique feature of *Plekha7* that distinguishes it from the other major AJ components studied—cadherins, catenins, nectins, afadin. The latter AJ components, as revealed by transcriptome analyses or IF

studies, are found both at the apical AJ belt and on spot-like AJs of APs, BPs, and neurons (Wilsch-Bräuninger et al., 2016), that is, throughout the developing cortical wall (Hirano and Takeichi, 2012; Fietz et al., 2012; Florio et al., 2015). In contrast, we find *Plekha7* to be virtually exclusively associated with the apical AJ belt of the embryonic mouse *Ncx*, in line with previous observations in non-neural tissues (Meng et al., 2008; Shah et al., 2016). This localization suggests that the function of *Plekha7* pertains to a specific feature of the apical AJ belt, rather than to the structure of AJs as such. It is intriguing to think that it is the belt nature that requires the presence of *Plekha7*, and that disruption of *Plekha7* expression facilitates the disassembly of the apical AJ belt into spot-like AJs, which then distribute along the lateral plasma membrane of NPCs in the process of delamination. A corollary of these considerations is that disruption of *Plekha7* expression does not interfere with the functionality of spot-like AJs, which in fact have been implicated in BP delamination by providing positional cues for basolateral primary cilia (Wilsch-Bräuninger et al., 2016).

Insm1 Induces NPC Delamination via Repression of *Plekha7* Expression

The analysis of *Insm1* and *Plekha7* mRNA levels in distinct NPC types strongly suggests that the repression of *Plekha7* expression by *Insm1* is indeed a cause underlying the BP delamination induced by *Insm1*. Specifically, our analysis of a previously published genome-wide transcriptome dataset of isolated NPC subpopulations (Florio et al., 2015) reveals that the level of *Plekha7* mRNA in *Tis21::GFP⁺* prominin-1⁺ NPCs is only about half of that in *Tis21::GFP⁻*, prominin-1⁺ NPCs (Figure S7B). In contrast to the latter NPC subpopulation, which comprises proliferative aRG, the former NPC subpopulation consists not only of aRG that generate BPs, but also of nascent BPs that have not yet delaminated from the VS and apical AJ belt (Florio et al., 2015). As delaminated BPs exhibit barely detectable *Plekha7* mRNA levels (Florio et al., 2015), these data imply that *Plekha7* expression is downregulated in nascent BPs. Moreover, the level of *Insm1* mRNA is ≈ 5 -fold higher in the *Tis21::GFP⁺* prominin-1⁺ NPCs than in the *Tis21::GFP⁻*, prominin-1⁺ NPCs (Figure S7A; Florio et al., 2015), suggesting that the upregulation of *Insm1* expression in BP-genic aRG and nascent BPs is the cause of the downregulation of *Plekha7* expression in the latter cells. Conversely, and consistent with the latter notion, our data mining of a previously published transcriptome dataset obtained with *Insm1* knockout mice (Osipovich et al., 2014) reveals that *Insm1* ablation increases the *Plekha7* mRNA level.

Plekha7 FE provided support for a functional link between *Insm1*-mediated *Plekha7* repression and NPC delamination. Specifically, co-expression of *Plekha7* along with *Insm1* was able to partially revert the *Insm1*-induced NPC delamination. Furthermore, *Plekha7* FE impeded the intrinsic NPC delamination, which likely involves the action of endogenous *Insm1*. Based on these findings, we conclude that *Insm1* induces NPC delamination via repression of *Plekha7* expression.

The latter conclusion, however, does not exclude the possibility that other genes, the expression of which is altered by *Insm1*, may also contribute to the *Insm1*-induced NPC delamination.

Thus, we found that *Insm1* FE in APs results in the repression of ninein, a protein that is associated with the apically tethered centrosomes and the knockdown of which has previously been shown to lead to increased NPC delamination (Wang et al., 2009) (Figure S7C). Furthermore, *Insm1* FE resulted in an increased expression of *scratch2* and *FoxP4*, two transcription factors that have also been found to promote NPC delamination via repression of AJ components, that is, cadherins (Rousso et al., 2012; Itoh et al., 2013) (Figure S7C).

The differences between the *Insm1* mRNA and *Insm1* protein levels in the lineage from *Tis21::GFP⁻* aRG to *Tis21::GFP⁺* aRG to nascent not yet delaminated BPs to delaminated BPs in the VZ to BPs in the SVZ deserve comment. The present and previous (Farkas et al., 2008; Florio et al., 2015) data indicate that the *Insm1* mRNA level, while low in the *Tis21::GFP⁻* aRG, increases substantially in the *Tis21::GFP⁺* aRG and even further in the subsequent cell states of the above-mentioned mouse lineage. In contrast, as shown in the present study, the *Insm1* protein becomes detectable, at a relatively high level, first in the nascent not yet delaminated BPs, with its level declining in the delaminated BPs in the VZ and SVZ. The presence of *Insm1* mRNA, but not *Insm1* protein, in *Tis21::GFP⁺* aRG is reminiscent of the discrepancy between *Tbr2* mRNA and *Tbr2* protein levels in these cells, which has been proposed to reflect microRNA-mediated inhibition of *Tbr2* mRNA translation (Florio et al., 2015). In this context, it is interesting to note that the 3' UTR of the *Insm1* mRNA contains a number of predicted binding sites for microRNAs, including those implicated in the inhibition of *Tbr2* mRNA translation (Florio et al., 2015).

Implications of the *Insm1*-Induced NPC Delamination for the Evolutionary Expansion of the *Ncx*

Our findings have several implications for the evolutionary expansion of the *Ncx*, notably regarding (1) the increase in the SVZ/VZ ratio as one of the underlying causes of this expansion and (2) the type of BP produced. First, we found that the highest levels of INSM1 protein in fetal human *Ncx* were detected in newborn BPs in the VZ, about half of which expressed the radial glia marker HOPX. This newborn BP-specific expression pattern of INSM1 matched that observed in the embryonic mouse *Ncx*, where some of the newborn *Insm1*-expressing BPs were still found to be attached to the VS. Together, these observations make it likely that *Insm1* exerts an NPC delamination-promoting role in fetal human *Ncx*, as is the case for embryonic mouse *Ncx*. If so, *Insm1* would constitute a key player in the generation and growth of the human SVZ, which is thought to underlie *Ncx* expansion.

Second, we demonstrate that *Insm1* FE induces mouse aRG to delaminate and to become bRG that retain a basal process and express the canonical radial glia marker *Sox2*. These findings are likely of relevance for the generation of bRG in fetal human *Ncx*. In fact, human bRG have been observed to arise from aRG directly by delamination (Gertz et al., 2014). Hence, the underlying mechanism of *Insm1*-induced NPC delamination in embryonic mouse *Ncx* uncovered in the present study, that is, triggering the disassembly of the apical AJ belt by repression of key components such as *Plekha7*, may serve

as a paradigm for the generation of bRG from aRG in fetal human Ncx.

Third, whereas the *Insm1*-induced NPC delamination clearly involved disengagement from the apical AJ belt, it did not affect the basal contact of the NPC, that is, the retention of its basal process and its interaction with the basal lamina. The latter features are characteristic of bRG and distinguish this BP type from bIPs (Florio and Huttner, 2014). In line with this, we observed a substantial proportion of *Insm1*⁺ cells in the VZ of fetal human Ncx that were *Tbr2*⁻, consistent with them being newborn bRG. Moreover, bRG, specifically, have been implicated in the evolutionary expansion of the Ncx and Ncx folding (Lui et al., 2011; Florio and Huttner, 2014; Fernández et al., 2016). Hence, the ability of *Insm1* to induce NPC delamination by selective disengagement from the apical AJ belt without interference with basal process-mediated basal lamina contact endows this transcription factor with an effectiveness that appears highly relevant for the evolutionary expansion of the Ncx.

STAR★METHODS

Detailed methods are provided in the online version of this paper and include the following:

- KEY RESOURCES TABLE
- CONTACT FOR REAGENT AND RESOURCE SHARING
- EXPERIMENTAL MODEL AND SUBJECT DETAIL
 - Mice
 - Human Tissue
- METHOD DETAILS
 - Plasmids
 - RNAs
 - Preparation of Recombinant Cas9 Protein/gRNA Complexes
 - *In Vitro* Cas9 Activity Test
 - In Utero Electroporation of Plasmids
 - In Utero Electroporation of Recombinant Cas9 Protein/gRNA Complexes
 - Organotypic Slice Culture
 - Microinjection of Organotypic Slices
 - Live Imaging
 - Transfection of EpH4-Ev Cells
 - FACS
 - RNA-Seq
 - Tissue Fixation and Sectioning
 - Immunofluorescence
 - Electron Microscopy
 - Image Acquisition
- QUANTIFICATION AND STATISTICAL ANALYSIS
 - Image Quantification
 - Transcriptome Data Processing and Analysis
 - Neocortical Cell Type Gene Enrichment Analysis
 - Neocortical Zone Gene Enrichment Analysis
 - Plekha7 Isoforms Analysis
 - Functional Group Analysis
 - *Insm1* Binding Analysis to the Plekha7 Gene Locus
- DATA AND SOFTWARE AVAILABILITY

SUPPLEMENTAL INFORMATION

Supplemental Information includes seven figures, one table, and two movies and can be found with this article online at <https://doi.org/10.1016/j.neuron.2018.01.052>.

ACKNOWLEDGMENTS

We thank C. Birchmeier for kindly providing the anti-*Insm1* antibody, and J.F. Fei, T.Y. Lin, and E. Tanaka for the kind donation of pCAG-EGFP and pCAG-EGFPnls plasmids, and P. Wimberger for kindly providing human fetal neocortical tissue. We are grateful to the services and facilities of the MPI-CBG for the outstanding support provided, notably J. Helppi and his team from the Animal Facility, I. Nüsslein and her team from the FACS Facility, M. Sarov and his team from the Genome Engineering Facility, J. Peychl and his team from the Light Microscopy Facility, and H. Brandl from the Scientific Computing Facility. We thank K. Long, F. Mora-Bermúdez, as well as other members of the Huttner laboratory for critical discussion. W.B.H. was supported by grants from the Deutsche Forschungsgemeinschaft (DFG) (SFB 655, A2), the European Research Council (250197), and ERA-NET NEURON (MicroKin).

AUTHOR CONTRIBUTIONS

Conceptualization, S.T., J.T.M.L.P., and W.B.H.; Formal Analysis, S.T.; Investigation, S.T., E.T., N.K., C.H., T.N., and M.W.-B.; Resources, A.D.; Writing – Original Draft, S.T. and W.B.H.; Writing – Review & Editing, S.T. and W.B.H.; Visualization, ST; Supervision, J.T.M.L.P. and W.B.H.; Project Administration, W.B.H.; Funding Acquisition, W.B.H.

DECLARATION OF INTERESTS

The authors declare no competing interests.

Received: June 9, 2017

Revised: December 28, 2017

Accepted: January 30, 2018

Published: March 1, 2018

REFERENCES

- Chiang, C., and Ayyanathan, K. (2013). Snail/Gfi-1 (SNAG) family zinc finger proteins in transcription regulation, chromatin dynamics, cell signaling, development, and disease. *Cytokine Growth Factor Rev.* 24, 123–131.
- Das, R.M., and Storey, K.G. (2014). Apical abscission alters cell polarity and dismantles the primary cilium during neurogenesis. *Science* 343, 200–204.
- Farkas, L.M., Haffner, C., Giger, T., Khaitovich, P., Nowick, K., Birchmeier, C., Pääbo, S., and Huttner, W.B. (2008). Insulinoma-associated 1 has a panneurogenic role and promotes the generation and expansion of basal progenitors in the developing mouse neocortex. *Neuron* 60, 40–55.
- Fernández, V., Llinares-Benadero, C., and Borrell, V. (2016). Cerebral cortex expansion and folding: What have we learned? *EMBO J.* 35, 1021–1044.
- Fietz, S.A., Lachmann, R., Brandl, H., Kircher, M., Samusik, N., Schröder, R., Lakshmanaperumal, N., Henry, I., Vogt, J., Riehn, A., et al. (2012). Transcriptomes of germinal zones of human and mouse fetal neocortex suggest a role of extracellular matrix in progenitor self-renewal. *Proc. Natl. Acad. Sci. USA* 109, 11836–11841.
- Florio, M., and Huttner, W.B. (2014). Neural progenitors, neurogenesis and the evolution of the neocortex. *Development* 141, 2182–2194.
- Florio, M., Albert, M., Taverna, E., Namba, T., Brandl, H., Lewitus, E., Haffner, C., Sykes, A., Wong, F.K., Peters, J., et al. (2015). Human-specific gene ARHGAP11B promotes basal progenitor amplification and neocortex expansion. *Science* 347, 1465–1470.
- Gertz, C.C., Lui, J.H., LaMonica, B.E., Wang, X., and Kriegstein, A.R. (2014). Diverse behaviors of outer radial glia in developing ferret and human cortex. *J. Neurosci.* 34, 2559–2570.

- Hirano, S., and Takeichi, M. (2012). Cadherins in brain morphogenesis and wiring. *Physiol. Rev.* *92*, 597–634.
- Itoh, Y., Moriyama, Y., Hasegawa, T., Endo, T.A., Toyoda, T., and Gotoh, Y. (2013). Scratch regulates neuronal migration onset via an epithelial-mesenchymal transition-like mechanism. *Nat. Neurosci.* *16*, 416–425.
- James, V., Zhang, Y., Foxler, D.E., de Moor, C.H., Kong, Y.W., Webb, T.M., Self, T.J., Feng, Y., Lagos, D., Chu, C.Y., et al. (2010). LIM-domain proteins, LIMD1, Ajuba, and WTIP are required for microRNA-mediated gene silencing. *Proc. Natl. Acad. Sci. USA* *107*, 12499–12504.
- Jia, S., Ivanov, A., Blasevic, D., Müller, T., Purfürst, B., Sun, W., Chen, W., Poy, M.N., Rajewsky, N., and Birchmeier, C. (2015). *Insm1* cooperates with *Neurod1* and *Foxa2* to maintain mature pancreatic β -cell function. *EMBO J.* *34*, 1417–1433.
- Kalebic, N., Taverna, E., Tavano, S., Wong, F.K., Suchold, D., Winkler, S., Huttner, W.B., and Sarov, M. (2016). CRISPR/Cas9-induced disruption of gene expression in mouse embryonic brain and single neural stem cells in vivo. *EMBO Rep.* *17*, 338–348.
- Kwon, G.S., and Hadjantonakis, A.K. (2007). Eomes:GFP—a tool for live imaging cells of the trophoblast, primitive streak, and telencephalon in the mouse embryo. *Genesis* *45*, 208–217.
- Lui, J.H., Hansen, D.V., and Kriegstein, A.R. (2011). Development and evolution of the human neocortex. *Cell* *146*, 18–36.
- Marie, H., Pratt, S.J., Betson, M., Eppe, H., Kittler, J.T., Meek, L., Moss, S.J., Troyanovsky, S., Attwell, D., Longmore, G.D., and Braga, V.M. (2003). The LIM protein Ajuba is recruited to cadherin-dependent cell junctions through an association with alpha-catenin. *J. Biol. Chem.* *278*, 1220–1228.
- Meng, W., Mushika, Y., Ichii, T., and Takeichi, M. (2008). Anchorage of microtubule minus ends to adherens junctions regulates epithelial cell-cell contacts. *Cell* *135*, 948–959.
- Niola, F., Zhao, X., Singh, D., Castano, A., Sullivan, R., Lauria, M., Nam, H.S., Zhuang, Y., Benezra, R., Di Bernardo, D., et al. (2012). Id proteins synchronize stemness and anchorage to the niche of neural stem cells. *Nat. Cell Biol.* *14*, 477–487.
- Nola, S., Daigaku, R., Smolarczyk, K., Carstens, M., Martin-Martin, B., Longmore, G., Bailly, M., and Braga, V.M. (2011). Ajuba is required for Rac activation and maintenance of E-cadherin adhesion. *J. Cell Biol.* *195*, 855–871.
- Nowakowski, T.J., Pollen, A.A., Sandoval-Espinosa, C., and Kriegstein, A.R. (2016). Transformation of the radial glia scaffold demarcates two stages of human cerebral cortex development. *Neuron* *91*, 1219–1227.
- O’Leary, N.A., Wright, M.W., Brister, J.R., Ciufo, S., Haddad, D., McVeigh, R., Rajput, B., Robbertse, B., Smith-White, B., Ako-Adjei, D., et al. (2016). Reference sequence (RefSeq) database at NCBI: current status, taxonomic expansion, and functional annotation. *Nucleic Acids Res.* *44* (D1), D733–D745.
- Osipovich, A.B., Long, Q., Manduchi, E., Gangula, R., Hipkens, S.B., Schneider, J., Okubo, T., Stoeckert, C.J., Jr., Takada, S., and Magnuson, M.A. (2014). *Insm1* promotes endocrine cell differentiation by modulating the expression of a network of genes that includes *Neurog3* and *Ripply3*. *Development* *141*, 2939–2949.
- Paridaen, J.T., Wilsch-Bräuninger, M., and Huttner, W.B. (2013). Asymmetric inheritance of centrosome-associated primary cilium membrane directs ciliogenesis after cell division. *Cell* *155*, 333–344.
- Platt, R.J., Chen, S., Zhou, Y., Yim, M.J., Swiech, L., Kempton, H.R., Dahlman, J.E., Parnas, O., Eisenhaure, T.M., Jovanovic, M., et al. (2014). CRISPR-Cas9 knockin mice for genome editing and cancer modeling. *Cell* *159*, 440–455.
- Rikitake, Y., Mandai, K., and Takai, Y. (2012). The role of nectins in different types of cell-cell adhesion. *J. Cell Sci.* *125*, 3713–3722.
- Roussou, D.L., Pearson, C.A., Gaber, Z.B., Miquelajauregui, A., Li, S., Portera-Cailliau, C., Morrisey, E.E., and Novitsch, B.G. (2012). Foxp-mediated suppression of N-cadherin regulates neuroepithelial character and progenitor maintenance in the CNS. *Neuron* *74*, 314–330.
- Sako-Kubota, K., Tanaka, N., Nagae, S., Meng, W., and Takeichi, M. (2014). Minus end-directed motor KIFC3 suppresses E-cadherin degradation by recruiting USP47 to adherens junctions. *Mol. Biol. Cell* *25*, 3851–3860.
- Shah, J., Guerrero, D., Vasileva, E., Sluysmans, S., Bertels, E., and Citi, S. (2016). PLEKHA7: cytoskeletal adaptor protein at center stage in junctional organization and signaling. *Int. J. Biochem. Cell Biol.* *75*, 112–116.
- Taverna, E., Haffner, C., Pepperkok, R., and Huttner, W.B. (2011). A new approach to manipulate the fate of single neural stem cells in tissue. *Nat. Neurosci.* *15*, 329–337.
- Taverna, E., Götz, M., and Huttner, W.B. (2014). The cell biology of neurogenesis: toward an understanding of the development and evolution of the neocortex. *Annu. Rev. Cell Dev. Biol.* *30*, 465–502.
- Taverna, E., Mora-Bermúdez, F., Strzyz, P.J., Florio, M., Icha, J., Haffner, C., Norden, C., Wilsch-Bräuninger, M., and Huttner, W.B. (2016). Non-canonical features of the Golgi apparatus in bipolar epithelial neural stem cells. *Sci. Rep.* *6*, 21206.
- Wang, X., Tsai, J.W., Imai, J.H., Lian, W.N., Vallee, R.B., and Shi, S.H. (2009). Asymmetric centrosome inheritance maintains neural progenitors in the neocortex. *Nature* *461*, 947–955.
- Wilsch-Bräuninger, M., Florio, M., and Huttner, W.B. (2016). Neocortex expansion in development and evolution - from cell biology to single genes. *Curr. Opin. Neurobiol.* *39*, 122–132.

STAR★METHODS

KEY RESOURCES TABLE

REAGENT or RESOURCE	SOURCE	IDENTIFIER
Antibodies		
Guinea pig anti-Insm1	Jia et al., 2015	N/A
Chicken anti-Tbr2	Millipore	Cat# AB15894, RRID: AB_10615604
Rabbit anti-Pax6	Covance Research Products	Cat# PRB-278P-100, RRID: AB_291612
Rabbit anti-Tbr2	Abcam	Cat# ab23345, RRID: AB_778267
Rabbit anti-Tbr2	Abcam	Cat# ab183991, RRID: AB_2721040
Rabbit anti-Tbr1	Abcam	Cat# ab31940, RRID: AB_220021
Goat anti-Ngn2	Santa Cruz Biotechnology	Cat# sc-19233, RRID: AB_2149513
Rat anti-RFP (it recognizes also mCherry)	Chromotek	Cat# 5f8-100, RRID: AB_2336064
Rabbit anti Phospho-H3 (Ser10)	Millipore	Cat# 06-570, RRID: AB_310177
Rat anti-Phospho-H3 (Ser28)	Abcam	Cat# ab10543, RRID: AB_2295065
Rabbit anti- γ -tubulin	Sigma-Aldrich	Cat# T5192, RRID: AB_261690
Mouse anti- γ -tubulin	Sigma-Aldrich	Cat# T6557, RRID: AB_477584
Rabbit anti-Plekha7	Sigma-Aldrich	Cat# HPA038610, RRID: AB_10671746
Mouse anti-p120-catenin	BD Biosciences	Cat# 610134, RRID: AB_397537
Mouse anti-Pancadherin	Sigma-Aldrich	Cat# C1821, RRID: AB_476826
Mouse anti-afadin	BD Biosciences	Cat# 610732, RRID: AB_398055
Rabbit anti-Hopx	Santa Cruz Biotechnology	Cat# sc-30216, RRID: AB_2120833
Mouse anti-TuJ1	Covance Research Products	Cat# MMS-435P, RRID: AB_2313773
Chicken anti-GFP	Aves Labs	Cat# GFP-1020, RRID: AB_10000240
Rabbit anti-GFP	Abcam	Cat# ab6556; RRID: AB_305564
Rabbit anti-RFP (it recognizes also mCherry)	Molecular Probes	Cat# R10367, RRID: AB_2315269
Rabbit anti-Arl13b	Proteintech Group	Cat# 17711-1-AP, RRID: AB_2060867
Mouse Anti-Dextran	STEMCELL Technologies	Cat# 60026, RRID: AB_2651016
Goat anti-Chicken IgY (H+L) Secondary Antibody, Alexa Fluor 488	Thermo Fisher Scientific	Cat# A-11039, RRID: AB_2534096
Alexa Fluor 488 AffiniPure Donkey Anti-Chicken IgY (IgG) (H+L) antibody	Jackson ImmunoResearch	Cat# 703-545-155, RRID: AB_2340375
Goat anti-Guinea Pig IgG (H+L) Highly Cross-Adsorbed Secondary Antibody, Alexa Fluor 488	Thermo Fisher Scientific	Cat# A-11073, RRID: AB_2534117
Donkey anti-Rabbit IgG (H+L) Highly Cross-Adsorbed Secondary Antibody, Alexa Fluor 488	Thermo Fisher Scientific	Cat# A-21206, RRID: AB_2535792
Cy3 AffiniPure Donkey Anti-Guinea Pig IgG (H+L)	Jackson ImmunoResearch	Cat# 706-165-148, RRID: AB_2340460
Goat anti-Guinea Pig IgG (H+L) Highly Cross-Adsorbed Secondary Antibody, Alexa Fluor 555	Thermo Fisher Scientific	Cat# A-21435, RRID: AB_2535856
Goat anti-Rat IgG (H+L) Cross-Adsorbed Secondary Antibody, Alexa Fluor 555	Thermo Fisher Scientific	Cat# A-21434, RRID: AB_2535855
Donkey anti-Rabbit IgG (H+L) Highly Cross-Adsorbed Secondary Antibody, Alexa Fluor 555	Thermo Fisher Scientific	Cat# A-31572, RRID: AB_162543
Alexa Fluor 647 AffiniPure Donkey Anti-Guinea Pig IgG (H+L)	Jackson ImmunoResearch	Cat# 706-605-148, RRID: AB_2340476
Goat anti-Guinea Pig IgG (H+L) Highly Cross-Adsorbed Secondary Antibody, Alexa Fluor 647	Thermo Fisher Scientific	Cat# A-21450, RRID: AB_141882
Goat anti-Rat IgG (H+L) Cross-Adsorbed Secondary Antibody, Alexa Fluor 647	Thermo Fisher Scientific	Cat# A-21247, RRID: AB_141778

(Continued on next page)

Continued

REAGENT or RESOURCE	SOURCE	IDENTIFIER
Donkey anti-Rabbit IgG (H+L) Highly Cross-Adsorbed Secondary Antibody, Alexa Fluor 647	Thermo Fisher Scientific	Cat# A-31573, RRID: AB_2536183
Donkey anti-Mouse IgG (H+L) Highly Cross-Adsorbed Secondary Antibody, Alexa Fluor 647	Thermo Fisher Scientific	Cat# A-31571, RRID: AB_162542
Goat anti-Chicken IgY (H+L) Secondary Antibody, Alexa Fluor 647	Thermo Fisher Scientific	Cat# A-21449, RRID: AB_2535866
Donkey anti-Goat IgG (H+L) Cross-Adsorbed Secondary Antibody, Alexa Fluor 647	Thermo Fisher Scientific	Cat# A-21447, RRID: AB_2535864
Goat anti Rabbit IgG 10 nm Gold	BBI solutions	Cat# EM.GAR10
Goat anti Rabbit IgG 5 nm Gold	BBI solutions	Cat# EM.GAR5
Bacterial and Virus Strains		
One Shot TOP10 Chemically Competent <i>E. coli</i>	Thermo Fisher Scientific	Cat# C404010
Biological Samples		
16 wpc human fetal neocortical tissue	Novogenix Laboratories	N/A
11 wpc human fetal neocortical tissue	Universitätsklinikum Carl Gustav Carus Dresden	N/A
Chemicals, Peptides, and Recombinant Proteins		
Cas9 WT protein, Injection ready, lyophilized	ToolGen	Cat# TGEN_CP1
Critical Commercial Assays		
Agencourt AMPure XP	Beckman Coulter	Cat# A63880
esiSCRIBE – <i>In Vitro</i> Transcription Kit	Eupheria Biotech	Cat# T7-esiSCRIBE-100
NEBNext for Illumina	New England Biolabs	Cat# E7370L
SMART-Seq v4 Ultra Low Input RNA Kit for Sequencing	Clontech	Cat# 634888
Neural Tissue Dissociation Kit (P)	Miltenyi Biotec	Cat# 130-092-628
mMESSAGE mMACHINE T7 Transcription Kit	Thermo Fisher Scientific	Cat# AM1344
Deposited Data		
Insm1 differentially expressed genes	This paper	GEO: GSE109709
Mouse and human neocortical cell types	Florio et al., 2015	GEO: GSE65000
Mouse and human neocortical zones	Fietz et al., 2012	GEO: GSE38805
Insm1 ChIP-seq	Jia et al., 2015	GEO: GSE54046
Experimental Models: Cell Lines		
EpH4-Ev	ATCC	Cat# ATCC CRL-3063; RRID: CVCL_S648
Experimental Models: Organisms/Strains		
Mouse: C57BL/6J0laHsd	Envigo	N/A
Mouse: C57BL/6JRj	Janvier Labs	N/A
Mouse: <i>Tg(Eomes::GFP)</i>	GENSAT Consortium and Kwon and Hadjantonakis, 2007	N/A
Oligonucleotides		
<i>LacZ</i> gRNA: TGCGAATACGCCACGCGAT	Kalebic et al., 2016	N/A
<i>Plekha7</i> gRNA1: TCGGAGGAACCTTAATGTTCCGG	This paper	N/A
<i>Plekha7</i> gRNA2: GAACCTTAATGTTCCGGTGGTGG	This paper	N/A
<i>Plekha7</i> gRNA3: AACATTAAGGTTCTCCGAATGG	This paper	N/A
<i>Plekha7</i> gRNA4: TAAGGTTCTCCGAATGGCCTGG	This paper	N/A
<i>Plekha7</i> gRNA5: AAACCAAAGACCGTCCAGCATGG	This paper	N/A
Primer for amplification <i>Plekha7</i> exons 5 and 6: <i>Plekha7</i> Fwd TTTGGGTGTCCTGAAGCAC	This paper	N/A
Primer for amplification <i>Plekha7</i> exons 5 and 6: <i>Plekha7</i> Rev GCCTGCCGCAAAGAAATTCT	This paper	N/A

(Continued on next page)

Continued		
REAGENT or RESOURCE	SOURCE	IDENTIFIER
Multiple cloning sites sequence gcatgcatgagctcgccgcgcctcgaccggtggcgcgccgatccaattggctagcgaattc	This paper	N/A
Recombinant DNA		
pCAG-Insm1-IRES-mCherry	This paper	N/A
pCAG-IRES-mCherry	This paper	N/A
pCAG-Plekha7-IRES-mCherry	This paper	N/A
pCAG-Insm1-IRES-GFPnls	This paper	N/A
pCAG-IRES-GFPnls	This paper	N/A
pCAG-mCherry	Paridaen et al., 2013	N/A
pCS2-GAP43GFP	Paridaen et al., 2013	N/A
pCAG-GFP	Florio et al., 2015	N/A
pCas9-Plekha7	ATUM	Cat# pD1321-AD
pCas9-LacZ	ATUM	Cat# pD1321-AD
pTNT-mRFP	Taverna et al., 2011	N/A
pCAG-GFPnls	Elly Tanaka Lab	N/A
pCMV-Sport6-Insm1	Source BioScience	Cat# IRAVp968B06165D, Clone Accession: BC051240
Software and Algorithms		
cutadapt	Python Software Foundation	RRID: SCR_011841
DAVID	LIB	RRID: SCR_001881
DESeq2	Bioconductor	RRID: SCR_015687
Fiji (Is Just ImageJ)	Fiji	RRID: SCR_002285
IGV	Broad Institute	RRID: SCR_011793
iTEM software	Olympus	N/A
Prism	GraphPad Software	RRID: SCR_002798
R	The R Foundation	N/A
TopHat	Johns Hopkins Univ./ Washington Univ.	RRID: SCR_013035
ZEN	Carl Zeiss	RRID: SCR_013672

CONTACT FOR REAGENT AND RESOURCE SHARING

Further information and requests for resources and reagents should be directed to Wieland B. Huttner (huttner@mpi-cbg.de).

EXPERIMENTAL MODEL AND SUBJECT DETAIL

Mice

All animal experiments were performed in accordance with German animal welfare laws and were overseen by the Institutional Animal Welfare Officer. Mice were maintained in specific pathogen-free conditions in the animal facility. C57BL/6JOLA^{Hsd} and the *Tg(Eomes::GFP)* mice were housed and bred in the MPI-CBG animal facility. The C57BL/6JRJ mice were bred in St. Berthevin Cedex by Janvier Labs and housed in the MPI-CBG animal facility for at least a week before any experiment.

Human Tissue

Human fetal neocortical tissue (11 wpc) was obtained from the Klinik und Poliklinik für Frauenheilkunde und Geburtshilfe, Universitätsklinikum Carl Gustav Carus of the Technische Universität Dresden, following elective pregnancy termination and informed written maternal consent, and with approval of the local University Hospital Ethical Review Committee. Gestational age was assessed by ultrasound measurements.

Human fetal neocortical tissue (16 wpc) was obtained from Novogenix Laboratories, following informed consent of the mother and elective termination. Gestational age was assessed by ultrasound measurements.

METHOD DETAILS

Plasmids

All DNA plasmids were extracted and purified using QIAprep Spin Miniprep kit (QIAGEN) or EndoFree Plasmid Maxi kit (QIAGEN) following the manufacturer's instructions. pCAG-*Insm1*-IRES-mCherry was cloned starting from the pCAG backbone of pCAG-GFP (a kind donation by Ji-Feng Fei and Elly Tanaka). The GFP coding sequence was removed using *NheI* and *EcoRI* restriction enzymes (New England Biolabs). The coding sequence for *Insm1* and mCherry, and the sequence for IRES, were PCR-amplified from the pCMV-Sport6-*Insm1*, pCAG-mCherry and pIRES2-eGFP plasmids, respectively. The *Insm1* "coding sequence" included, in addition to the true coding sequence from the ATG until the stop codon, 25 bp of the 5'UTR. The fragments were subsequently ligated using Gibson Assembly Master Mix (New England Biolabs) following the manufacturer's instructions. Afterward, the DNA was purified using QIAquick PCR Purification Kit (QIAGEN), eluted in 5 μ L of distilled water and subsequently used to transform competent bacteria cells.

pCAG-IRES-mCherry was generated starting from pCAG-*Insm1*-IRES-mCherry. The *Insm1* coding sequence was substituted by a multiple cloning site using *SphI* and *EcoRI* restriction enzymes (New England Biolabs). pCAG-Plekha7-IRES-mCherry was generated starting from pCAG-IRES-mCherry. Mouse Plekha7 isoform 1 cDNA was amplified by PCR from a E15.5 BL6/J mouse brain cDNA library, and the blunt PCR product was ligated into the pCR-Blunt II-TOPO vector (Zero Blunt TOPO PCR Cloning Kit, Thermo Fisher Scientific). The pCR Blunt II TOPO-Plekha7 vector was then digested with *EcoRI* and *SmaI* restriction enzymes (New England Biolabs) and subcloned into the *EcoRI* site of pCAG-IRES-mCherry. pCAG-*Insm1*-IRES-GFPnls was generated starting from pCAG-*Insm1*-IRES-mCherry. The mCherry coding sequence was removed using *Clal* and *BsrGI* restriction enzymes (New England Biolabs). The GFP coding sequence with a C-terminal nuclear localization signal (GFPnls) was amplified from the pCAG-EGFPnls (kind donation by Tzi-Yang Lin and Elly Tanaka). pCAG-*Insm1*-IRES and GFPnls were ligated using Gibson Assembly Master Mix (New England Biolabs) following the manufacturer's instructions. The DNA was purified using QIAquick PCR Purification Kit (QIAGEN), eluted in 5 μ L of distilled water and used to transform competent bacteria cells. pCAG-IRES-GFPnls was generated starting from pCAG-*Insm1*-IRES-GFPnls. The *Insm1* coding sequence was substituted by a multiple cloning sites using *SphI* and *EcoRI* restriction enzymes (New England Biolabs).

RNAs

The *mRFP* mRNA was generated as described in Taverna et al. (2011).

To generate the *Insm1* mRNA, the pCMV-Sport6-*Insm1* plasmid was linearized using *XcmI* or *NotI* (New England Biolabs), capped and polyadenylated using the T7 mMESSAGE-mMACHINE kit. The *Insm1* mRNA was dissolved in RNase-free water at 0.8 μ g/ μ L and snap-frozen as 1-2 μ L aliquots.

All gRNAs were prepared as described in Kalebic et al. (2016).

Preparation of Recombinant Cas9 Protein/gRNA Complexes

The preparation of recombinant Cas9 protein/gRNA complexes was done as described in Kalebic et al. (2016) with minor modifications. Recombinant Cas9 protein (1 μ g/ μ L) was incubated for 15 min at 37°C with either *LacZ* gRNA (0.33 μ g/ μ L) (Platt et al., 2014) or with *Plekha7* gRNA4 and gRNA5 (0.167 μ g/ μ L each).

In Vitro Cas9 Activity Test

The *in vitro* Cas9 activity test was done as described in Kalebic et al. (2016) with minor modifications. All gRNAs were tested using a 1.2 kb PCR-amplified template spanning both exons 5 and 6 of the *Insm1* gene. The template was amplified using the primers *Plekha7 Fwd* and *Plekha7 Rev*.

In Utero Electroporation of Plasmids

Pregnant mice carrying E12.5, E13.5 or E.14.5 embryos were anesthetized using isofluorane, and the indicated plasmid DNA together with 0.25% Fast Green FCF (Sigma) in PBS was injected into the lateral ventricles of the embryos, followed by a series of pulses (32 V, 6x 50 ms-pulses with 1 s intervals). The final concentrations of plasmids were as follows: pCAG-*Insm1*-IRES-mCherry 0.6 – 0.8 μ g/ μ L; pCAG-mCherry 0.4 – 0.6 μ g/ μ L; pCS2-GAP43GFP 0.5 – 1.2 μ g/ μ L; pCas9-Plekha7 2.5 μ g/ μ L; p Cas9-LacZ 2.5 μ g/ μ L; pCAG-Plekha7-IRES-mCherry 2.5 μ g/ μ L; pCAG-IRES-mCherry 1.5 μ g/ μ L; pCAG-*Insm1*-IRES-GFPnls 0.5 – 1.2 μ g/ μ L; pCAG-IRES-GFPnls 1 μ g/ μ L. The pregnant mice were sacrificed either 12 hr, 24 hr or 48 hr after *in utero* electroporation (IUE) for IF, 24 hr after IUE for FACS-isolation and RNA-seq, or right after surgery for the time-lapse live imaging experiments, and the embryos were processed as described below.

For experiments with a short-term survival (12 hr), *Insm1*-encoding plasmid and the corresponding control were co-electroporated with either the membrane-tagged GFP or the GFP plasmids to allow the identification of targeted brains before embedding.

For the time-lapse live imaging experiments, *Insm1*-encoding plasmid and the corresponding control were co-electroporated with the membrane-tagged GFP plasmid.

For forced co-expression of *Plekha7* and *Insm1*, pCAG-*Insm1*-IRES-GFPnls (0.5 μ g/ μ L) was co-electroporated at a 1/4 molar ratio with either pCAG-Plekha7-IRES-mCherry (2.5 μ g/ μ L) or pCAG-IRES-mCherry (1.5 μ g/ μ L, control).

In Utero Electroporation of Recombinant Cas9 Protein/gRNA Complexes

Surgery was performed as indicated above with minor modifications, and the protocol was adapted from [Kalebic et al. \(2016\)](#). Prior to surgery, 0.1% Fast Green FCF and the pCAG-GFP plasmid (0.25 $\mu\text{g}/\mu\text{L}$) were added to the recombinant Cas9 protein (0.8 $\mu\text{g}/\mu\text{L}$) complexed either to gRNA *LacZ* (0.25 $\mu\text{g}/\mu\text{L}$) or to *Plekha7* gRNA4 and gRNA5 (0.132 $\mu\text{g}/\mu\text{L}$ each).

Organotypic Slice Culture

Organotypic slices were prepared and cultured as described in [Taverna et al. \(2011\)](#). Briefly, organotypic slices were embedded at room temperature in collagen type I-A and transferred into a 35 mm Glass Bottom Microwell dish. The slices were placed for 5 min at 37°C, followed by 40 min in slice culture medium to allow for the solidification of the collagen, before adding 2 mL of slice culture medium.

Microinjection of Organotypic Slices

Tissue was processed as described previously ([Taverna et al., 2011](#)). After dissection and removal of the meninges, brains were embedded in 3% low melting point agarose, and organotypic slices with a thickness of 250–300 μm were prepared using a vibratome.

Microinjection of mRNA into single aRG in organotypic slice culture was performed as described in [Taverna et al. \(2011\)](#). The microinjection solutions included dextran (3.3 $\mu\text{g}/\mu\text{L}$) and *mRFP* RNA (0.4 $\mu\text{g}/\mu\text{L}$) with or without *Insm1* RNA (0.4 $\mu\text{g}/\mu\text{L}$). Microinjection of recombinant Cas9 protein with gRNA was performed as described in [Kalebic et al. \(2016\)](#). The microinjection solutions included dextran (2.2 $\mu\text{g}/\mu\text{L}$) and recombinant Cas9 protein (0.66 $\mu\text{g}/\mu\text{L}$) complexed either to gRNA *LacZ* (0.22 $\mu\text{g}/\mu\text{L}$) or to *Plekha7* gRNA4 and gRNA5 (0.11 $\mu\text{g}/\mu\text{L}$ each). After microinjection, organotypic slices were kept for 24 hr in the slice culture chamber maintained at 37°C in a humidified atmosphere of 40% O₂/5% CO₂/55% N₂, before fixation.

Live Imaging

Organotypic slices were prepared as described above. Time-lapse live imaging of NPC behavior in organotypic slice culture was performed as described previously ([Paridaen et al., 2013](#)) with minor modifications. Movies were taken with a Zeiss 710 Multiphoton Laser Scanning Microscope equipped with a tunable pulsed Ti-Sapphire laser tuned to 900 nm and with a Zeiss LD C-Apochromat 40x 1.1 NA long-distance water objective, heated using an objective heater. Z stacks of 100 μm with a Z step-size of 0.8 μm and a pixel size of 0.18 μm were acquired every 10–15 min for a time range of 10–35 hr after IUE.

Transfection of Eph4-Ev Cells

Eph4-Ev cells were seeded into 6-well plates and co-transfected using Lipofectamine 3000 (Thermo Fisher Scientific) following the manufacturer's instructions. The final amounts of each plasmid per well were as follows: pCAG-GFP 1 μg ; pCas9-Plekha7 4 μg ; pCas9-LacZ 4 μg ; pCAG-Plekha7-IRES-mCherry 630 ng; pCAG -IRES-mCherry 500 ng. For *Plekha7* gene disruption experiments, cells were re-plated on coverslips into 24-well plates one day after transfection and processed for analysis 3 days later. For *Plekha7* FE, cells were processed for analysis 2 days after transfection.

FACS

Tissue was processed as described previously ([Florio et al., 2015](#)) with minor modifications. Cerebral cortices of electroporated embryos were processed to obtain a cell suspension using the Neural Tissue Dissociation Kit (P). Cortices were incubated with the pre-warmed papain-containing enzyme mix 1 (950 μL Buffer X + 5 μL Enzyme P) for 15 min at 37°C on a rotating platform. The suspension was then incubated with the papain inhibitor-containing enzyme mix 2 (10 μL Buffer Y + 5 μL Enzyme A) for 10 min at 37°C on a rotator. Samples were dissociated by gently pipetting up and down with a P-1000 pipette to obtain a single-cell suspension, centrifuged at 300 g for 3 min, and resuspended in 400 μL of pre-warmed Tyrode's solution.

The BD FACSAria II cell sorter was treated with RNaseZap RNase decontamination solution prior to use. Prior to cell sorting, the cell suspensions prepared from mouse embryonic neocortex upon either control or *Insm1* FE were passed through a 40- μm pore size filter. For each experiment, 10,000 cells from untreated cortices were used to set the voltage parameters and all gates. Live cells were identified based on the cell size using the side scatter (SSC)/forward scatter (FSC) plot (P1 gate) and then the SSC-Width (W)/SSC-Area (A) plot (P2 gate). The P2 population was then analyzed and sorted according to the mCherry fluorescence, using a 561-nm laser and a 610/20 bandpass filter (P3 gate, SSC linear/PE-Texas Red exponential plot). 5000 cells were sorted for each condition in 150 μL of RTL plus lysis buffer (RNeasy Plus Micro Kit, QIAGEN) with 1% of 2-mercaptoethanol, briefly vortexed, centrifuged in a small tabletop centrifuge and stored at –80°C until RNA extraction.

RNA-Seq

Cells were subjected to RNA extraction using RNeasy Plus Micro Kit (QIAGEN) according to the manufacturer's instructions. mRNA amplification, library preparation and sequencing were performed as described in ([Florio et al., 2015](#)).

Tissue Fixation and Sectioning

Tissue was fixed in either 1% or 4% paraformaldehyde in 120 mM phosphate buffer pH 7.4 for 2–5 hr at room temperature and then overnight at 4°C on a shaker. In the case of IF with the anti-Plekha7 antibody, tissue was fixed in 0.5% paraformaldehyde in 120 mM

phosphate buffer pH 7.4 for 30 min at room temperature, prior to being processed for cryosectioning. Fixed tissue was sectioned to obtain either 20- μm cryosections or 50- μm vibratome sections.

EpH4-Ev cells were washed twice with PBS and fixed with 1% PFA in phosphate buffer for 5 min at room temperature, followed by immunofluorescence as described below.

Immunofluorescence

IF on either cryosections or vibratome sections was performed as described in (Taverna et al., 2011; Paridaen et al., 2013) with minor modifications. If necessary, sections were incubated in antigen retrieval solution (10 mM sodium citrate buffer pH 6.0) for 1–1.5 hr at 70°C. For the IF of 11 wpc human fetal neocortex with antibodies against *Insm1* and *Hopx*, sections were incubated in antigen retrieval solution for 1 hr at 80°C. For the IF of 11 wpc human fetal neocortex with antibodies against *Insm1* and *Tbr2*, sections were incubated in 10 mM sodium citrate buffer pH 6.0 containing 0.05% Tween-20 for 1 hr at 80°C. Sections were permeabilized with 0.3% Triton X-100 for up to 1 hr, quenched with 0.1 M glycine in PBS for 30 min and incubated with blocking solution (0.2% gelatin, 300 mM NaCl, 0.3% Triton X-100 in PBS) for 30 min at room temperature. Sections were then incubated with the primary antibodies diluted in blocking solution for a minimum of one night to a maximum of a week at 4°C, depending on the antibody used. The incubation with fluorophore-conjugated secondary antibodies (diluted 1:500) and DAPI was carried out for 1–2 hr at room temperature.

IF of EpH4-Ev cells was performed as described above with minor modification. Cells were incubated with a fetal calf serum-based blocking solution (FCS buffer; 5% FCS, 0.3% Triton X-100 in PBS) for 30 min at room temperature, followed by incubation with primary antibodies diluted in FCS buffer for 3 days at 4°C.

Primary antibodies were used at the following dilutions: guinea pig anti-*Insm1* 1:500–1:1000; chicken anti-*Tbr2* 1:500; rabbit anti-*Pax6* 1:300; rabbit anti-*Tbr2* 1:250; rabbit anti-*Tbr1* 1:500; goat anti-*Ngn2* 1:25; rat anti-RFP 1:500; rabbit anti-RFP 1:1000; rabbit anti-phosphoH3 1:300; rat anti-phosphoH3 1:300; rabbit anti- γ -tubulin 1:500; mouse anti- γ -tubulin 1:250; rabbit anti-*Plekha7* 1:200–1:300; mouse anti-afadin 1:250; mouse anti-p120-catenin 1:300; mouse anti-pan-cadherin 1:500; chicken anti-GFP 1:1000; rabbit anti-*Arl13b* 1:500; rabbit anti-GFP 1:1000; rabbit anti-*Hopx* 1:100; mouse anti-*Tuj1* 1:500.

Electron Microscopy

Electron microscopy was performed as described previously (see references in Wilsch-Bräuninger et al., 2016). The primary antibody against *Plekha7* was used at a 1:50–1:100 dilution, and the secondary antibody against rabbit IgG at a 1:30 dilution.

Image Acquisition

Fluorescence images were acquired using an LSM 780 NLO with GaAsP detector or an LSM 880 Airy single point scanner confocal microscope using 40x and 63x objectives. Images were taken as either 1- μm (40x) or 0.8- μm (63x) single optical sections. In case of images taken as tile scans, the stitching was performed using the ZEN software.

QUANTIFICATION AND STATISTICAL ANALYSIS

Image Quantification

Quantifications were done on single optical sections, except for the quantification of abventricular centrosomes in the VZ which was done using the maximum intensity projection (MIP) of 3 optical sections. The quantification of time-lapse movies was done following the delaminating cells in each frame using both single optical sections and 3D reconstruction. All quantifications of embryonic mouse neocortex were done in the medial position along the rostro-caudal axis, and in the dorsolateral region along the dorsoventral axis.

Quantification of abventricular centrosomes in the VZ. The electroporated area was identified by mCherry IF. Abventricular centrosomes in the VZ were quantified in a 100 μm -wide microscopic field. Centrosomes were scored as abventricular when located at least 15 μm basal to the ventricular surface.

Quantification of *Plekha7* IF. *Plekha7* IF was quantified at the apical AJs of mCherry+ cells. The quantification was done on 8-bit images and measured as mean gray value of a 2- μm high rectangular area having the width equal to the width of the apical endfoot. Each data point is the mean of two consecutive but non-overlapping 1- μm optical sections.

Quantification of time-lapse movies. Delaminating GFP+ cells were scored as bIPs if (i) they did not show apically directed nuclear migration prior to the retraction of the plasma membrane from the ventricular surface (i.e., delamination), (ii) they exhibited an only short basal process, if any, prior to delamination, and (iii) they adopted a multipolar morphology after delamination. Delaminating GFP+ cells were scored as aRG→bRG if (i) they showed apically directed nuclear migration prior to delamination (provided that they could be observed sufficiently early), (ii) they exhibited a long basal process (extending beyond VZ and SVZ) prior to delamination, and (iii) they retained a radial morphology after delamination.

Quantification of the presence and absence of apical contact after microinjection. The quantification was done as previously described (Taverna et al., 2011) with minor modifications. The contours of targeted cells were traced using either mRFP or dextran IF. Together with the presence of an apical centrosome, the contours were used to determine the presence or absence of an apical contact at the ventricular surface.

Quantification of the presence of a basal process after microinjection. The contours of targeted cells were traced using either mRFP or dextran. Delaminated, radially aligned mRFP+ or dextran+ cells were scored for the presence or absence of a basal process with a length $\geq 25 \mu\text{m}$.

Quantification of Plekha7 and afadin IF in GFP+ neighboring EpH4-Ev cells after transfection. IF was quantified at the apical AJs, defined as the structure with the strongest afadin IF at the border between two cells. The quantification was done on 8-bit images and measured as mean gray value of a $0.6\text{-}\mu\text{m}$ long line perpendicular to the afadin staining and centered on the peak of afadin IF.

All quantifications were done using Fiji. Statistical significance was determined using either Mann–Whitney U test, unpaired Student's t test, Fisher's exact test or Chi-square test. Unpaired Student's t test was used only if the data passed normality test (Shapiro-Wilk normality test or Kolmogorov-Smirnov test). The difference was assumed significant when $p < 0.05$. Data visualization and statistical analysis were conducted using Prism.

Transcriptome Data Processing and Analysis

Reads of the same sample on different sequencing lanes were combined and subjected to adaptor trimming using cutadapt. The processed reads were aligned to the mouse reference genome (mm10/ GRCm38) using TopHat. The following table summarizes the information about the quality of the RNA-seq data:

Sample	Median base quality	Number of reads	Number of mapped reads	Mapping efficiency
Ctrl_1	38	65281236	55079656	84
Ctrl_2	38	29153233	24873705	85
Ctrl_3	38	54212847	46128152	85
Insm1_1	38	57642508	45725605	79
Insm1_2	38	52513848	44055926	84
Insm1_3	38	59382178	49529537	83

Genes of the Ensembl release 61 were processed using Cuffdiff2. The expression of each gene was expressed as FPKM value, and a gene was considered not expressed if the average value in three independent experiments was lower than 1 FPKM in both Insm1 FE and control samples. Differential expression was determined without distinguishing between splice variants of the gene under study and using all protein-coding genes as transcriptome reference. Differentially expressed genes were defined using a cutoff of adjusted p value < 0.05 . The statistical analysis as well as the calculation of the numbers of differentially expressed genes in the various sectors of the Volcano plot were calculated using R. GO term enrichment analyses and functional annotation clustering of the differentially expressed genes were performed using DAVID applying a cutoff of Expression Analysis Systematic Explorer (EASE) > 2 . Data visualization was performed using R and Prism.

Neocortical Cell Type Gene Enrichment Analysis

The analysis was performed using a pre-existing RNA-seq dataset (Florio et al., 2015). The Insm1 differentially expressed genes were divided into two subgroups:

- Genes downregulated upon Insm1 FE (Insm1 downregulated genes, 406 genes in total)
- Genes upregulated upon Insm1 FE (Insm1 upregulated genes, 233 genes in total)

For each subgroup, enrichment in one or more neocortical cell type or subtype was determined using a hyper-geometric test with a cut-off of adjusted p value < 0.01 . Cell type and subtype gene expression was defined as follows, using original cut-off published by (Florio et al., 2015):

- Proliferative aRG (aRG-P) – genes that are significantly more highly expressed in this cell subtype compared to neurogenic aRG;
- Neurogenic aRG (aRG-N) – genes that are significantly more highly expressed in this cell subtype compared to proliferative aRG;
- aRG – genes that are significantly more highly expressed in this cell type compared to bIPs, bRG and neurons (N);
- bIPs and bRG – genes that are significantly more highly expressed in at least one of these two cell types compared to aRG and N;
- N – genes that are significantly more highly expressed in this cell type compared to aRG, bIPs and bRG.

The enrichment score was calculated with the following formula: $-\log_{10}(\text{adjusted p value})$. All analyses were performed using R and data visualization was performed using Prism.

Neocortical Zone Gene Enrichment Analysis

The analyses were performed using a pre-existing RNA-seq dataset (Fietz et al., 2012). The *Insm1* differentially expressed genes were divided into two subgroups as described above. For each subgroup, enrichment in one or more neocortical zone was determined using a hyper-geometric test with a cut-off of adjusted p value < 0.01. Only protein-coding genes were taken into account. The original dataset was analyzed for differentially expressed genes using DESeq2 with a cut-off of adjusted p value < 0.05, with definitions as follows:

- Mouse VZ – genes that are significantly more highly expressed in this zone compared to mouse SVZ and CP;
- Mouse SVZ – genes that are significantly more highly expressed in this zone compared to mouse VZ and CP;
- Mouse CP – genes that are significantly more highly expressed in this zone compared to mouse VZ and SVZ;
- Human VZ – genes that are significantly more highly expressed in this zone compared to human SVZ and CP;
- Human SVZ – genes that are significantly more highly expressed in this zone compared to human VZ and CP;
- Human CP – genes that are significantly more highly expressed in this zone compared to human VZ and SVZ.

For the analysis of neocortical zones in the human dataset, only genes with a mouse ortholog were considered. The enrichment score was calculated with the following formula: $-\log_{10}(\text{adjusted p value})$. All analyses were performed using R and data visualization was performed using Prism.

Plekha7 Isoforms Analysis

Isoform tracking of a previously published transcriptome dataset (Fietz et al., 2012) and of our transcriptome dataset was performed using cuffdiff2. Resulting abundance estimates were compared using R and data visualization was performed using Prism.

Functional Group Analysis

The function of the 48 genes common to the four groups was analyzed using published literature and the Universal Protein Resource.

Insm1 Binding Analysis to the Plekha7 Gene Locus

The *Insm1* binding analysis was performed using a previously published ChIP-seq dataset and the peak-scores and peak-widths reported therein (Jia et al., 2015). The *Plekha7* gene locus was analyzed for the presence of ChIP-seq peaks using the IGV software.

DATA AND SOFTWARE AVAILABILITY

The accession number for the *Insm1* differential expressed genes reported in this paper is GEO: GSE109709.